Exact joint distributions of three global characteristic times for Brownian motion

Alexander K. Hartmann[1] and Satya N. Majumdar[2]

[1]*Institut für Physik, Universität Oldenburg, D-26111 Oldenburg, Germany*
[2]*LPTMS, CNRS, Univ. Paris-Sud, Université Paris-Saclay, 91405 Orsay, France*

We consider three global chracteristic times for a one-dimensional Brownian motion $x(\tau)$ in the interval $\tau \in [0,t]$: the occupation time $t_{\rm o}$ denoting the cumulative time where $x(\tau) > 0$, the time $t_{\rm m}$ at which the process achieves its global maximum in $[0,t]$ and the last-passage time t_l through the origin before t. All three random variables have the same marginal distribution given by Lévy's arcsine law. We compute exactly the pairwise joint distributions of these three times and show that they are quite different from each other. The joint distributions display rather rich and nontrivial correlations between these times. Our analytical results are verified by numerical simulations.

I. INTRODUCTION

Whenever measurements on physical [1], economical [2], biological [3] or other systems are performed, one is always limited in the amount of data one can obtain, let it be due to financial, time or fundamental physical constraints. It is then beneficial to have available additional data about correlations or even the joint distributions involving at least two relevant quantities, either from previous measurements or on the basis of modeling. This is of crucial interest if one quantity is easier to determine such that costly measurements of the other quantity can be avoided or reduced. For disease diagnosis, it is often easy to access risk factors which allow to restrict expensive or even dangerous medical examinations to persons with a high disease probability. For example, osteoporosis [4] is a very common chronic disease but has no obvious early symptoms. Still, a significant height loss is a predictor for osteoporosis [5–7], such that expensive and incriminating X-ray examinations can be restricted only to high-risk patients. As another example, the investigation of geological structures [8] is of high interest, e.g., to measure the water content or to find other important resources below the surface. These structures can be obtained most accurately by invasive methods like core samples obtained from drilling. On the other hand, seismic measurements allow for a much simpler investigation and correlate well with results from more expensive methods [9, 10]. Similarly, seismic reflection data can be used to predict promising places for much more costly investigations by archaeological excavation [11].

This idea of offsetting the lack of resources in measuring one observable via exploiting its correlation with another less expensive observable is of general interest in any stochastic time series. For example, the time series may represent the amplitude of earthquakes in a specific seismic region, the amount of yearly rainfall in a given area, the temperature records in a given weather station, or the price of a stock over a given period t. While the marginal distributions of single quantities can be computed for many time series [12], there are very few results on the joint distributions of two observables associated to a time series. The simplest and the most ubiquitous stochastic time series represents the position of a one- dimensional Brownian motion (BM) of a given duration t, or its discrete-time analogue of a one-dimensional random walk [13, 14], with applications in Physics and Chemistry [15], Electrical Engineering [16], Economics [17, 18] or Social Sciences [19]. This is a paradigmatic toy model of a correlated time series where many observables can be computed analytically and hence has been extensively used to test various general physical ideas [13, 20–23]. In this model, the joint distribution of local (in time) observables, e.g. of the positions at two different times can be easily computed and is simply a bivariate Gaussian distribution. However, computing the joint distribution between two global (in time) observables is nontrivial even in this simple toy model, since it involves the full history of the trajectory over the interval $[0,t]$. For example, the joint distribution of the global maximal value $M(t)$ and the time $t_{\rm m} \equiv t_{\rm max}$ at which it occurs in $[0,t]$ can computed exactly with many different applications [24–31]. Another example consists in computing exactly the joint distibution of $t_{\rm m}$ and $t_{\rm min}$ (time at which the global minimum occurs) [32, 33]. This is clearly of interest in finance, because one would like to buy a stock at time $t_{\rm min}$ and sell it at $t_{\rm max}$.

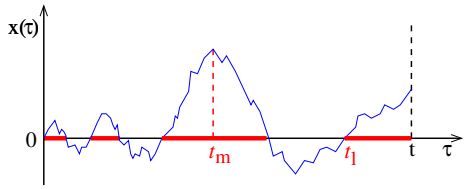

FIG. 1. A schematic trajectory of a Brownian motion $x(\tau)$ that starts at $x(0) = 0$ and evolves up to time t. Also the last-passage time $t_{\rm l}$ and the time of the maximum $t_{\rm m}$ are shown. The occupation time $t_{\rm o}$ is the sum of the red intervals on the time axis where $x(\tau) > 0$.

In this paper, we consider three global quantitites for a time series of duration t starting at the origin. They are respectively (i) the occupation time $t_{\rm o} = \int_0^t \theta(x(\tau))\, d\tau$, i.e., the cumulative time where $x(\tau) > 0$ with $\theta(z)$ denoting the Heaviside step function: $\theta(z) = 1$ for $z > 0$ and $\theta(z) = 0$ for $z < 0$ (ii) the time $t_{\rm m}$ of the maximum $\max_\tau x(\tau)$ in $[0,t]$, and (iii) the time $t_{\rm l}$ of the last passage, before t, of the process to $x = 0$ (see Fig. 1). All three observables are random variables each supported over $[0,t]$. For example, for a time series representing the value of a stock over a maturity period $[0,t]$, normalized to the value when bought, the occupation time is the time where it exhibits profit, the time of the maximum is the best time to sell, and the last-passage time indicates the last time the value changes from profit to loss or

vice-versa. For a Brownian time series, the marginal distributions of these random varibles were computed by Lévy [34] and quite remarkably, they all follow the same *arcsine law* $p_i(t_i|t) = 1/\left[\pi\sqrt{t_i(t-t_i)}\right]$ for $t_i = t_{\rm o}, t_{\rm m}$ or $t_{\rm l}$, where the name originates from the corresponding arcsine cumulative distribution, i.e., $\text{Prob.}[t_i \leq T|t] = (2/\pi)\,\sin^{-1}\left(\sqrt{T/t}\right)$.

These three quantities are relevant in various complex systems and have been studied a for a wide variety of stochastic processes with diverse applications. The occupation time $t_{\rm o}$ has been analyzed, e.g., for random jump processes [35], renewal and resetting processes [36–39], Gaussian Markov processes [40, 41] and has played an important role in the context of persistence in nonequilibrium systems [23, 42–45]. Furthermore, it has been studied for various other processes such as opinions in voter models [46], blinking nanacrystals [47], diffusion in a disordered environment [48–51], a class of spin glass models [52], sub- and superdiffusive processes [53–56], random acceleration process [57], active run-and-tumble process [58–60], permutation genrated random walks [61] and for a noninteracting Brownian gas [62]. Experimentally, the occupation time has been studied for colloidal quantum dots [63, 64], thermodynamic currents [65], and coherently driven optical resonators [66].

The time $t_{\rm m}$ at which the global maximum occurs in a process of total duration t has been studied extensively in the context of extreme-value statistics [22, 67, 68]. Examples include Brownian motion with drift [24, 25, 28], permutation-generated random walks [61], Brownian and anomalous diffusion with constraints [26, 27, 30, 69, 70], random acceleration process [71], heterogeneous diffusion [55, 72], run-and-tumble process [58, 70], fractional Brownian motion [56, 73], processes with stochastic resetting [70, 74]. The lack of symmetry of the distribution of $t_{\rm m}$ around its mean $t/2$ in a stationary time series has been shown to be a sufficient condition that the underlying dynamics violates detailed balance [70, 75]. Another application of t_m of a 1-d process is to estimate the mean perimeter and the mean area of the convex hull of a 2-d process [76–82]. Other applications appear in finance [28, 83, 84] and sports [85].

The last-passage time $t_{\rm l}$ has been studied also for diffusion in extermal potentials [86, 87], in imhomogeneous environement [55], and in permutation-generated random walks [61]. For applications, it was considered for electronic ring oscillators [88, 89] and for investigating fission [90]. It has been used for setting up Monte Carlo methods to calculate capacitances on systems with flat or spherical surfaces [91, 92]. The last-passage time has also been applied to devise optimal inspection policies of degrading systems [93] and in finance [94].

Although the marginal distributions of these three global quantities $t_{\rm o}$, $t_{\rm m}$ and $t_{\rm l}$ have been studied for various stochastic time series as mentioned above, their mutual correlations, encoded in pairwise joint distributions, have not been studied to the best of our knowledge. As an example why these joint distributions are of interest, one could consider animal movement as a toy application. The development of low-orbiting micro satellites like the KITSUNE 6U satellite [95] makes the observation with high-temporal imaging possible

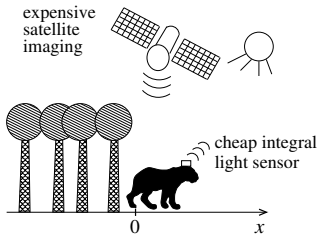

FIG. 2. An animal living in a mixed habitat consisting of forests and open grass land ($x > 0$). Only for $x > 0$ it makes sense to use expensive stallite imaging. With a low-cost and low-weight light sensor an estimation of the time $t_{\rm o}$ the animal spends at $x > 0$ allows for better estimate times when to obtain expensive images.

such that in the future even animals can be observed, but at high cost. For example, tigers live in a mixed habitats consisting of deep woods and open grass land [96], see Fig. 2. Here, it makes only sense to buy expensive high-resolution satellite footings, for times the animal is in the open land. We assume that one has to decide which of the expensive images to buy before being able to look at them. Clearly, the best time footage to buy is the time $t_{\rm m}$ where the animal is maximally displaced from the wooded region so that it is completely visible. However, $t_{\rm m}$ is not known apriori and has a broad distribution $p(t_{\rm m}|t)$ distributed all over $[0, t]$ (as in the arcsine law for a one-dimensional Brownain motion). So, it is not clear which time or times to choose. However, suppose we have some knowledge about the occupation time $t_{\rm o}$ that corresponds to the cumulative time an animal spends in the open land. This could be measured easily with a low-cost and low-weight sensor which does not annoy the animal considerably, i.e., without relatively heavy GPS or time-stamping facilities. Conditioned on the knowledge of $t_{\rm o}$, a representative value of $t_{\rm m}$ with high probability may emerge and one can then buy the footage corresponding to that. We will show an explicit example of that for the 1-d Brownian motion later (in the right panel of Fig. 4). Thus, exploiting the correlations between two global quantities in a model, here for a simple random walk, allows for a much better targeted analysis of the data.

To gain better insights into the correlations between these three global quantities, one needs to compute the pairwise joint distributions of them analytically in a simple model time series. We have not seen any result in the literature on the joint distributons of these three global observables for any stochastic process, including even for the simple one-dimensional Brownian motion. This lack of benchmark results motivated us to study the joint bivariate distributions between these three observables for a one-dimensional Brownian motion of duration t, perhaps the simplest and most ubiquitous one-dimensional stochastic process. For this model, the marginal distributions of all three quantities are identically given by the arcsine law, as mentioned earlier. Here we compute exactly the pairwise joint distributions and demonstrate that, even in this simple model, they exhibit a rather rich, nontrivial, and unexpected behavior, not at all compatible with, say, standard linear correlations. We hope that the results and the methods presented in the paper will mark the starting point for comput-

ing and exploring these joint distributions for other stochastic processes as well.

The rest of the paper is organised as follows. In Section II we introduce the model and the three observables of interest more precisely. In Section III, we provide a brief outline of the derivations and also summarize our main results. Section IV contains a conclusion and discussion. Since the actually derivations of these results are somewhat technical, we relegate them to four Appendices.

II. MODEL AND OBSERVABLES OF INTEREST

The model stochastic process we study in this paper is perhaps the simplest, namely a one dimensional Brownian motion of duration t evolving via the Langevin equation

$$\frac{dx}{d\tau} = \sqrt{2D}\,\eta(\tau)\,, \tag{1}$$

where D is the diffusion constant and $\eta(\tau)$ is a Gaussian white noise with zero mean and delta correlator: $\langle \eta(\tau_1)\eta(\tau_2)\rangle = \delta(\tau_1-\tau_2)$. We assume that the process starts at the origin, i.e., $x(0)=0$.

The three classical observables of interest are last-passage time, occupation time and time of maximum, already introduced briefly in the introduction. Below we define them more precisely (see Fig. (1) for a schematic representation).

- **Last-passage time.** Let $t_{\rm l}$ denote that last time before t that the Brownian motion crosses the origin (from either side). Evidently $0 \le t_{\rm l} \le t$.

- **Occupation time.** This is the total time that the Brownian motion of duration t spends on the positive half axis, i.e.,

$$t_{\rm o} = \int_0^t \theta\left(x(\tau)\right)\, d\tau\,, \tag{2}$$

  where $\theta(x)$ is the standard Heaviside theta function: $\theta(x)=1$ for $x>0$ and $\theta(x)=0$ for $x<0$. Clearly $0 \le t_{\rm o} \le t$.

- **Time of the maximum.** We denote by $t_{\rm m}$ the time at which the Brownian motion achieves its maximum (on the positive side) within the interval $[0,t]$. Again, $0 \le t_{\rm m} \le t$.

These three observables are each supported over $[0,t]$ and they are random variables since they fluctuate from sample to another. The marginal distributions of these random variables were computed by Lévy [34] and it is well known that they all share the same probability distribution function (PDF). In fact, the three marginal PDF's, given the duration t, can be written in the scaling form

$$p_i\left(t_i|t\right) = \frac{1}{t}\, f\left(\frac{t_i}{t}\right)\,, \qquad \text{with} \quad 0 \le t_i \le t\,, \tag{3}$$

valid for all t, where $t_i = t_{\rm o}$, $t_{\rm m}$ or $t_{\rm l}$. The scaling function $f(x)$ is identical for all three observables and is given explicitly by

$$f(x) = \frac{1}{\pi\,\sqrt{x\,(1-x)}} \qquad \text{with} \quad 0 \le x \le 1\,. \tag{4}$$

Interestingly, the marginal distributions of all three observables $t_{\rm l}$, $t_{\rm o}$ and $t_{\rm m}$ are independent of the diffusion constant D of the Brownian motion. The cumulative distribution of each of them has the arcsine form: $\mathrm{Prob.}[x \le u] = \int_0^u f(x)\,dx = (2/\pi)\,\sin^{-1}\left[\sqrt{u}\right]$. Hence, these three laws are famously known as arcsine laws of Lévy [34].

One interesting fact about the marginal distribution $f(x)$ in Eq. (4) is that it has a U shape with peaks at the two end points $x=0$ and $x=1$. In other words, the typical values of x (where the PDF achieves its maximum value) do not coincide with the average $\langle x\rangle = \int_0^1 x\, f(x)\, dx = 1/2$. This is very different from the bell shaped curves whose peak coincides with its mean. For example, consider the observable $t_{\rm o}$ denoting the occupation time. Its scaled value $x=1$ means $t_{\rm o}=t$, i.e., it correesponds to paths that, starting at the origin, stay entirely on the positive side during $[0,t]$. On the other hand $x=0$, i.e., $t_{\rm o}=0$ corresponds to paths that, starting at the origin, stay entirely on the negative side during $[0,t]$. Thus, physically this U shaped curves indicate that the typical trajectories of a Brownian motion are 'stiff', i.e., if they deviate to the positive (negative) side, they tend to stay positive (negative) for the full interval $[0,t]$. These facts are, by no means, very intuitive even for this simple Brownain motion.

Furthermore, it is also not obvious at all why these three observables should have the same marginal distributions. While there exist probablistic equivalences between these observables using some special properties of Brownian motion [34], for a physicist it is not easy to follow these mathematical equivalences. The arcsine laws for these three observables have been derived in the physics literature using methods that are quite different for each observable. For example, the arcsine law for the occupation time $t_{\rm o}$ can be derived by using the Feynman-Kac method involving path-integrals [104]. On the other hand, the derivations of the arcsine laws for $t_{\rm m}$ and $t_{\rm l}$ involve path decomposition methods that involve spilitting the full trajectory into two parts: (i) the interval $[0,t_{\rm m}]$ prior to $t_{\rm m}$ (or for $t_{\rm l}$) and (ii) the interval $[t_{\rm m},t]$ after the occurrence of $t_{\rm m}$ (and similarly for $t_{\rm l}$). The probability weight of each part is then computed separately and then they are multipled (using the Markov property of the process) to get the full probability distribution of the observable $t_{\rm m}$ and $t_{\rm l}$. For a derivation of the arcsine law for $t_{\rm m}$ using this path decomposition method, see Ref. [27]. We also rederive these marginal laws later in the Appendices from our more general results on joint bivariate distributions of these three variables.

While the marginal PDF's of these fractions are identical, our goal here is to compute their bivariate joint distributions

$$\begin{aligned}
\mathrm{Prob.}\left[t_{\rm l},\, t_{\rm o}|\, t\right] &= P_{12}(t_{\rm l},\, t_{\rm o}|t)\,,\\
\mathrm{Prob.}\left[t_{\rm o},\, t_{\rm m}|t\right] &= P_{23}(t_{\rm o},\, t_{\rm m}|t)\,,\\
\mathrm{Prob.}\left[t_{\rm l},\, t_{\rm m}|t\right] &= P_{13}(t_{\rm l},\, t_{\rm m}|t)\,.
\end{aligned} \tag{5}$$

The subscripts 1, 2 and 3 refer respectively to t_1, t_o and t_m. On dimensional grounds, these three joint distributions can be expressed in the scaling form, valid for all t,

$$P_{12}(t_1,\, t_o|t) \;=\; \frac{1}{t^2}\,\mathcal{P}_{12}\left(\frac{t_1}{t},\,\frac{t_o}{t}\right),$$
$$P_{23}(t_o,\, t_m|t) \;=\; \frac{1}{t^2}\,\mathcal{P}_{23}\left(\frac{t_o}{t},\,\frac{t_m}{t}\right),$$
$$P_{13}(t_1,\, t_m|t) \;=\; \frac{1}{t^2}\,\mathcal{P}_{13}\left(\frac{t_1}{t},\,\frac{t_m}{t}\right). \qquad (6)$$

We will show that these three joint distributions are highly nontrivial and are rather different from each other. We compute them exactly using the ϵ-path decomposition method, first proposed in Refs. [97, 98] and then used subsequently in numerous other related problems [21, 27, 32, 33, 70, 75, 81, 99]. Below we outline the main ideas leading to the results and the details of the derivations are presented in the Appendices since they are a bit technical.

III. RESULTS

In this Section, we present the main results for the joint bivariate distributions of the three main observables and discuss their physical implications. We also briefly outline here the main ideas behind the derivations of these results, while leaving the technical details to the Appendices.

A. Last-passage time t_1 and occupation time t_o

First, we focus on computing the $P_{12}(t_1,\, t_o|t)$, because this is the simplest of the three. The idea is to first express the joint distribution as $P_{12}(t_1, t_o|t) = P_{\rm cond}(t_o|t_1, t)\, p_1(t_1|t)$ where $P_{\rm cond}(t_o|t_1, t)$ denotes the conditional distribution of t_o given t_1 and t, while $p_1(t_1|t)$ is the marginal distribution of t_1 given in Eq. (3). We split the total duration t into two intervals: (I) $0 \le \tau \le t_1$ and (II) $t_1 \le \tau \le t$. Consequently, t_o can also be split into two parts $t_o = t_o^{\rm I} + t_o^{\rm II}$, where the two random variables $t_o^{\rm I}$ and $t_o^{\rm II}$ are independent of each other, for a given fixed t_1. The idea then is to compute the PDF of each of them separately and then convolute them to compute the full conditional probability.

For the first interval, the Brownian motion starts at the origin at $\tau = 0$ and ends at the origin at $\tau = t_1$. This then corresponds to a *Brownian bridge* of duration t_1, starting and ending at the origin. We then need to compute the distribution of the occupation time $t_o^{\rm I}$ of this Brownian bridge of duration t_1. In fact, the occupation time for a Brownian bridge is a well studied object [13] and it is well known that the PDF of the occupation time $t_o^{\rm I}$ is flat, i.e., $p_{\rm I}(t_o^{\rm I}|t_1) = \frac{1}{t_1}\,\theta\left(t_1 - t_o^{\rm I}\right)$. This result can be understood intuitively as follows. Since a Brownian bridge will return to the origin after period t_1, one can take any time instant $\tau_0 \in [0, t_1]$ and consider the trajectory over $[\tau_0, \tau_0 + t_1]$ with an imposed periodicity $x(\tau) = x(\tau - t_1)$ for $\tau > t_1$. Subtracting $x(\tau_0)$ so that this new trajectory also goes from from origin to origin in time t_1, one has a new Brownian bridge configuration which has the same weight as the original one. However, the occupation time in this new configuration is quite different from the original one. Thus, one can generate any value of the occupation number by sliding and stiching the original trajectory appropriately, but all with equal weights. This leads to the fact all allowed values of occupation time are equally likely for a Brownian bridge.

Concerning the second interval, the process crosses zero for the last time at $\tau = t_1$, it may either cross from above or from below, each with equal probability $1/2$. For the first case, the process stays below zero, so $t_o^{\rm II} = 0$, in the other case we have $t_o^{\rm II} = (t - t_1)$. Thus, we obtain $p_{\rm II}(t_o^{\rm II}|t_1) = \frac{1}{2}\,\delta\left(t_o^{\rm II}\right) + \frac{1}{2}\,\delta\left(t_o^{\rm II} - (t - t_1)\right)$. The distribution for the total occupation time $t_o = t_o^{\rm I} + t_o^{\rm II}$ is given by the convolution $P_{\rm cond}(t_o|t_1, t) = \int_0^t dt_o^{\rm I}\, p_{\rm I}(t_o^{\rm I})\, p_{\rm II}(t_o - t_o^{\rm I})$. We then apply the arcsine result for the marginal distribution of t_1 from Eq. (3) and obtain a scaling form (see Appendix A for details)

$$P_{12}(t_1, t_o|t) = \frac{1}{t^2}\,\mathcal{P}_{12}\left(\frac{t_1}{t} = x,\,\frac{t_o}{t} = y\right), \qquad (7)$$

where the scaling function is given by

$$\mathcal{P}_{12}(x, y) \;=\; \frac{1}{2\,\pi\, x^{3/2}\,\sqrt{1-x}}\,[\theta(x-y) + \theta(x+y-1)]$$
$$\times\,\theta(1-x)\,\theta(1-y). \qquad (8)$$

The scaling function is plotted in Fig. 3. To obtain a better impression of the distribution, a cross section at $y = 1/4$ is also displayed on the right panel of Fig. 3.

Some features of the result for $\mathcal{P}_{12}(x, y)$ in Eq. (8) can be guessed/understood physically. For example, we see from Fig. 3 (both in the left and in the right panel) that $\mathcal{P}_{12}(x, y)$ vanishes unless the scaled last-passage time $x > y$ or $x > 1 - y$, i.e., $x > \min(y, 1 - y)$ for a given fixed scaled occupation time y. In other words the scaling function $\mathcal{P}_{12}(x, y)$ vanishes if $x < \min(y, 1 - y)$. For example, in the right panel of figure 3 where $y = 1/4$, we see that the joint PDF vanishes for $x < y = 1/4$. One can associate a physical picture to this result as follows. Consider the event when the last-passage through the origin before t where the trajectory crosses from the positive to the negative side. In this case the occupation time contribution from the interval $[t_1, t]$ is zero since the trajectory can not recross back to the positive side in $[t_1, t]$. Thus the occupation time has contribution only from the interval $[0, t_1]$ and consequently $t_o < t_1$, i.e., $x > y$. In other words, for a given x, we must have $y < x$ for $\mathcal{P}_{12}(x, y)$ to be nonzero. On the other hand, if the last-passage through the origin occurs from the negative to the positive side, the walker will spend the remaining time $t - t_1$ at positive positions, and might even have spent some time before the last-passage in the positive range. Thus, the occupation time must be equal to or larger than $t - t_1$, i.e., $y > 1 - x$. Hence, we must have $y > 1 - x$ for $\mathcal{P}_{12}(x, y)$ to be nonvanishing. Combining these two events, we then conclude (without doing any computation) that $\mathcal{P}_{12}(x, y)$ must be nonzero if and only if y does not belong to the interval $[x, 1 - x]$, or equivalently if $x > \min(y, 1 - y)$. Let us remark that this argument is rather

general, and is completely independent of the actual random process.

Of course, this argument does not provide us the amount of jump discontinuities at $x = y$ or $x = 1-y$ as seen, e.g., in the right panel of Fig. (3). The magnitudes of such discontinuities in the joint PDF do depend on the specific process and can be read off the exact formula in Eq. (8) for a Brownian motion. Also, for fixed y, we see from Eq. (8) that the scaling function diverges as $\mathcal{P}_{12}(x,y) \sim (1-x)^{-1/2}$ as $x \to 1$ (see also the right panel of Fig. (3)). This divergence as $x \to 1$ typically corresponds to paths that stay almost positive for their entire duration t, except for a little excursion to the origin and re-crossing it from below at time $t_{\rm l}$ for the last time. Also, notice that unlike the marginal arcsine law of $t_{\rm o}$, the joint PDF of $t_{\rm o}$, conditioned on a fixed $t_{\rm l}$, is not symmetric around its average value $\langle t_{\rm o}\rangle = t/2$. Let us make a cautionary remark here by emphasizing that all these little nice features of the joint PDF may be understood heuristicallly once we have the exact formula as in Eq. (8). But without such an exact formula, one will not be able to make such heuristic guesses very confidently.

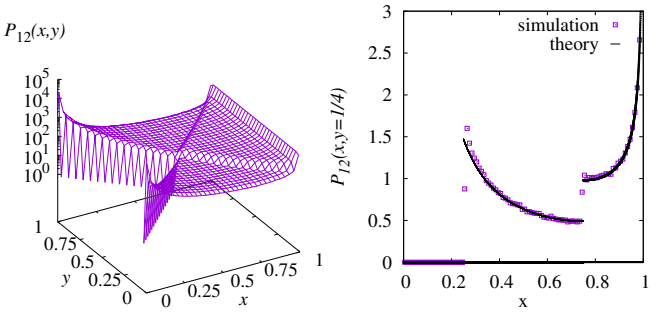

FIG. 3. (left) The scaled joint PDF $\mathcal{P}_{12}(x,y)$ of the fractions $x = t_{\rm l}/t$ and $y = t_{\rm o}/t$. (right) The distribution with fixed $y = 1/4$. The simulation results are shown by open symbols.

Here, also a comparison with numerical simulations of random walks is included. For that purpose, standard random walks, starting at zero, are performed with a certain number n_t of steps. Thus, the position at step n is given by $x(n) = \sum_1^n \eta(n)$, where $\eta(n)$'s are independently and identically distributed standard Gaussian increments, numerically drawn by using the Box-Muller approach [100]. The data can be scaled to any time span $[0,t]$ simply by rescaling the times to nt/n_t. This approximates Brownian motion with step size $\Delta t = t/n_t$. Here, we use $n_t = 10000$ and average over independent 10^8 walks. Note that only the signs of the positions $x(n)$ are important here, so no position rescaling is necessary. All three times $t_{\rm o}$, $t_{\rm l}$ and $t_{\rm m}$ can be directly read off from the time series $x(n)$ and used to create corresponding joint histograms. The accuracy is limited by the discretised sampling at resolution Δt, but this is sufficient for the present study, as visible in Fig. 3. For even better accuracy of $t_{\rm l}$ and $t_{\rm m}$, one could use adaptive interval splitting approaches [101].

Clearly, the joint distribution in (8) does not factorize demonstrating nontrivial correlations between the scaled variables $x = t_{\rm l}/t$ and $y = t_{\rm o}/t$, which we computed explicitly. Interestingly, while the first-order correlation vanishes $\langle xy\rangle - \langle x\rangle\langle y\rangle = 0$, higher order correlations are nonzero. For example, we find that x and y are weakly anticorrelated $\langle x^2y^2\rangle - \langle x^2\rangle\langle y^2\rangle = -7/384$, see Eq. (A17) in Appendix A, a result that is also confirmed numerically.

The first order correlation is zero, because for any path $\{x[n]\}$ in $[0,t]$, which has last-passage time $t_{\rm l}$ and occupation time $t_{\rm o}$, one has the path $\{-x[n]\}$ which has exactly the same last-passage time $t_{\rm l}$ and the 'opposite' occupation time $t - t_{\rm o}$. Since both paths have the same probability, the dependence between $t_{\rm l}$ and $t_{\rm o}$ averages out to zero. The observed higher-order anticorrelation between $t_{\rm o}$ and $t_{\rm l}$ has the following physical implication. It indicates that when $t_{\rm o}$ is large, typically $t_{\rm l}$ is small and vice versa. Now $t_{\rm o}$ large indicates paths that stay on the positive side for a long time and they seem to cross the origin quite early so that $t_{\rm l}$ is small. On the other hand, if $t_{\rm o}$ is small, the typical path stays on the negative side for a long time and crosses zero from the negative to the positive side only near the end of the time interval $[0,t]$, indicating that $t_{\rm l}$ is relatively large. Let us emphasize that such weak higher-order anticorrelations between $t_{\rm l}$ and $t_{\rm o}$ could not have been guessed without the explicit exact result in Eq. (8).

B. Occupation time $t_{\rm o}$ and time of maximum $t_{\rm m}$

Computing the joint distribution $P_{23}(t_{\rm o}, t_{\rm m}|t)$ turns out to be harder than computing $\mathcal{P}_{12}(t_{\rm l}, t_{\rm o}|t)$ in the previous subsection. Here the main idea is to first compute a more complicated object $P(t_{\rm o}, t_{\rm m}, M|t)$ denoting the joint distribution of $t_{\rm o}$, $t_{\rm m}$ and the value of the maximum M within the interval $[0,t]$. Once we know this, the joint distribution $P_{23}(t_{\rm o}, t_{\rm m}|t)$ can be computed by marginalising over M, i.e.,

$$P_{23}(t_{\rm o}, t_{\rm m}|t) = \int_0^\infty P(t_{\rm o}, t_{\rm m}, M|t)\, dM\,. \tag{9}$$

Now, this quantity $P(t_{\rm o}, t_{\rm m}, M|t)$ can be computed again by splitting the full trajectory into two parts: (i) left part over $[0, t_{\rm m}]$ where the trajectory propagates from $x(0) = 0$ to $x(t_{\rm m}) = M$ at time $t_{\rm m}$ and (ii) right part over $[t_{\rm m}, t]$ where the trajectory propagates from $x(t_{\rm m}) = M$ at time $t_{\rm m}$ to $x(t)$ at time t where the final position will be integrated over $[-\infty, M]$. The total occupation time $t_{\rm o}$ is again the sum of the occupation times of the left and the right intervals. The distribution of $t_{\rm o}$ is then the convolution of the possible values of $t_{\rm o}$ for the left and the right interval. Thus, one can formally write down $P(t_{\rm o}, t_{\rm m}, M|t)$ by multiplying the appropriate propagators of the left and the right intervals by adapting the Feynman-Kac method. The full computation eventually gives quite powerful and nontrivial result, but the derivation is rather technical and hence we present the details in Appendix B. The upshot at the end of the day is that this method gives us an exact formula for the triple Laplace transform of $P_{23}(t_{\rm o}, t_{\rm m}|t)$ with respect to $t_{\rm o}$, $t_{\rm t}$ and t, as given in Eq. (B2) in Appendix B. Unfortunately, this triple Laplace transform is very hard to invert explicitly. Consequently, unlike the scaled joint distributions $\mathcal{P}_{12}(x,y)$ and $\mathcal{P}_{13}(x,y)$, it is hard to obtain the scaled joint distribution $\mathcal{P}_{23}(x,y)$ explicitly. However, as

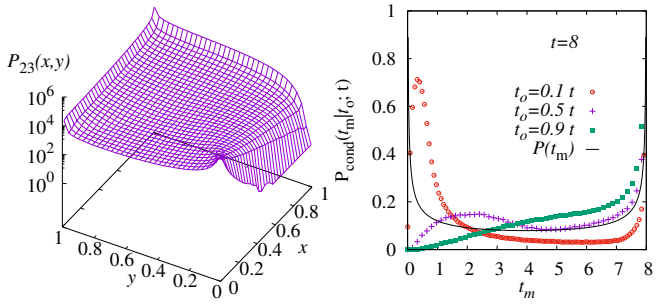

FIG. 4. (left) The scaled joint PDF $\mathcal{P}_{23}(x,y)$ of the fractions $x = t_{\rm o}/t$ and $y = t_{\rm m}/t$ plotted in the $(x-y)$ plane. (right) Corresponding distribution of the time $t_{\rm m} \in [0,t]$ (here $t = 8$) of the maximum position, conditioned to different values of the occupation time $t_{\rm o}$.

we will see in Appendix B, the triple Laplace transform does give explicit access to correlation moments between $t_{\rm o}$ and $t_{\rm m}$.

Indeed, from Eq. (B2) in Appendix B, we find that the two marginal distributions for $t_{\rm o}$ and $t_{\rm m}$ result in the arcsine laws, and also obtain various covariance functions explicitly. For example, we get

$$\begin{aligned}
\langle t_{\rm o}\, t_{\rm m}\rangle - \langle t_{\rm o}\rangle\, \langle t_{\rm m}\rangle &= \frac{11}{144}\, t^2 \\
\langle t_{\rm o}\, t_{\rm m}^2\rangle - \langle t_{\rm o}\rangle\, \langle t_{\rm m}^2\rangle &= \frac{43}{648}\, t^3 \\
\langle t_{\rm o}^2\, t_{\rm m}\rangle - \langle t_{\rm o}^2\rangle\, \langle t_{\rm m}\rangle &= \frac{509}{7200}\, t^3 \\
\langle t_{\rm o}^2\, t_{\rm m}^2\rangle - \langle t_{\rm o}^2\rangle\, \langle t_{\rm m}^2\rangle &= \frac{25997}{414720}\, t^4 \,, \qquad (10)
\end{aligned}$$

which are all compatible with our numerical results. The explicit results in (10) indicate that $t_{\rm o}$ and $t_{\rm m}$ are actually positively correlated, in contrast to the pair $(t_{\rm o}, t_{\rm l})$ which are anti-correlated. The positive correlation implies that if $t_{\rm o}$ is large then $t_{\rm m}$ is likely to be large and vice versa. This has the following physical implications. Consider a trajectory that has a large $t_{\rm o}$, i.e., it stays on the positive side for a long time. Then, for such a trajectory, the maximum is likely to occur at the end of the interval $[0,t]$ implying $t_{\rm m}$ to be relatively large. Similarly, if $t_{\rm o}$ is small, it corresponds to trajectories that spend most of their lifetime on the negative side. The positive correlations between $t_{\rm o}$ and $t_{\rm m}$ indiacte that for such trajectories the maximum will likely occur at earlier times such that $t_{\rm m}$ is small. Those paths start from the origin, go upwards to achieve their maximum at an early time with $t_{\rm m}$ small and then turn around, cross zero and stay negative till the final time t.

In Fig. 4, the scaled joint PDF $\mathcal{P}_{23}(x,y)$ obtained from the numerical simulations is shown. Here, no discontinuities are present, but for fixed value $x = t_{\rm o}/t$ of the scaled occupation time, the behavior of the probability changes considerably. For small scaled occupation times x, the distribution is large for small times y of the time of maximum, while for large occupation times $x \approx 1$ it is opposite. This is also visible in the distribution of $t_{\rm m}$ conditioned to a value of $t_{\rm o}$, as shown in the right panel of Fig. 4.

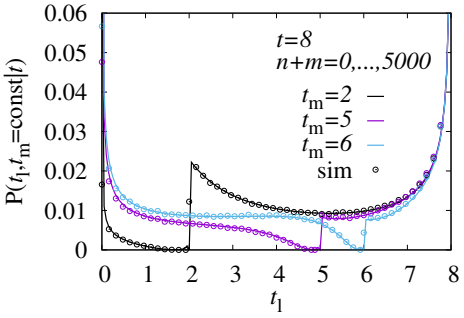

FIG. 5. The joint PDF $P_{13}(t_{\rm l}, t_{\rm m}|t)$ from numerically evaluating Eq. (12) with $t = 8$, shown as a function of $t_{\rm l}$ for three different fixed values of $t_{\rm m}$. Simulation results are shown as symbols.

C. Last-passage time $t_{\rm l}$ and time of maximum $t_{\rm m}$

In this subsection, we compute the joint bivariate distribution $P_{13}(t_{\rm l}, t_{\rm m}|t)$. As in the previous subsection, it turns out to be convenient to first consider a more complicated object, namely the joint distribution $P(t_{\rm l}, t_{\rm m}, M|t)$ of $t_{\rm l}$, $t_{\rm m}$ and the value M of the maximum up to time t. Upon obtaining this three variable joint distribution, one can obtain $P_{13}(t_{\rm l}, t_{\rm m}|t)$ via the marginalisation

$$P_{13}(t_{\rm l}, t_{\rm m}|t) = \int_0^\infty P(t_{\rm l}, t_{\rm m}, M|t)\, dM \,. \qquad (11)$$

The quantity $P(t_{\rm l}, t_{\rm m}, M|t)$ can be computed again via the path decomposition method as before by splitting a path into three intervals: $[0, t_{\rm l}]$, $[t_{\rm l}, t_{\rm m}]$ and $[t_{\rm m}, t]$ in the case when $t_{\rm l} < t_{\rm m}$. In the opposite case $t_{\rm m} < t_{\rm l}$ we split the path into intervals $[0, t_{\rm m}]$, $[t_{\rm m}, t_{\rm l}]$ and $[t_{\rm l}, t]$ respectively. The propagators of the path in the three intervals are calculated separately and then multiplied together to obtain the full joint distribution $P(t_{\rm l}, t_{\rm m}, M|t)$. Finally, using (11), we obtain the desired result for $P_{13}(t_{\rm l}, t_{\rm m}|t)$. Skipping details that can be found in Appendix C, we present our main result here. We get

$$P_{13}(t_{\rm l},t_{\rm m}|t) \;=\; \left[\frac{1}{\pi\, t_{\rm l}^{3/2}\,\sqrt{t-t_{\rm l}}}\sum_{n=0}^{\infty}\frac{(-1)^n}{(1+\alpha\, n^2)^{3/2}}\right]\theta(t_{\rm l}-t_{\rm m})+$$
$$+\;\left[\frac{1}{\pi\, t_{\rm l}^{2}}\sum_{n,m=0}^{\infty}\frac{(-1)^{(n-1)}\,n^2}{\gamma_{n,m}^{3/2}}\left[1-\left(1+2\,\pi\,\sqrt{\gamma_{n,m}}\right)\,e^{-2\,\pi\,\sqrt{\gamma_{n,m}}}\right]\right]\theta(t_{\rm m}-t_{\rm l})\,, \qquad (12)$$

with $\gamma_{n,m} = \frac{1}{t_{\rm l}}\left[n^2\,(t_{\rm m}-t_{\rm l})+(2m+1)^2\,(t-t_{\rm m})\right]$ and $\alpha = \frac{t_{\rm m}\,(t_{\rm l}-t_{\rm m})}{t_{\rm l}\,(t-t_{\rm l})}$. Let us remark that while this joint distribution is explicit and can be plotted (see below), it is very hard to calculate the moments and correlations between $t_{\rm l}$ and $t_{\rm m}$ from Eq. (12). At least, we were unable to do it and this remains an interesting future challenge. Also, even deriving the marginal arcsine laws for $t_{\rm l}$ and $t_{\rm m}$ from Eq. (12) is not obvious. However, one can check numerically that they do reproduce the arcsine laws for the marginals.

The adavantage of the explicit result in Eq. (12) is that it can be numerically evaluated and plotted. Indeed, we numerically evaluated the double sum in Eq. (12) using the `mpfr` library [102], for an arbitrary choice of $t = 8$, by summing all terms with $n + m \leq 5000$. In Fig. 5, we plot the resulting $P_{13}(t_{\rm l}, t_{\rm m}|t)$ as a function of $t_{\rm l}$ for three different fixed values of $t_{\rm m}$, and the simulation results for comparison. They match very well. For fixed values of $t_{\rm m}$ and t, the joint PDF $P_{13}(t_{\rm l}, t_{\rm m}|t)$, as a function of $t_{\rm l}$, exhibits a strong peak at $t_{\rm l} = 0$. This peak corresponds to paths that start at the origin, wander to the positive side, achieve their maximum at the given $t_{\rm m}$ and do not cross the origin further, so that the last-passage through the origin occurs essentially at the begining so that $t_{\rm l} = 0$.

In Fig. 5, one also observes a discontinuity of $P_{13}(t_{\rm l}, t_{\rm m}|t)$ as a function of $t_{\rm l}$ (for fixed $t_{\rm m}$ and t) . While $P_{13}(t_{\rm l}, t_{\rm m}|t)$ vanishes very fast as $t_{\rm l} \to t_{\rm m}$ from below, it approaches a nonzero constant when $t_{\rm l} \to t_{\rm m}$ from above. This can be understood as follows: For a given time $t_{\rm m}$ of maximum, the only possibility that the last passage at zero occurs slightly before the maximum is that the trajectory crosses zero in positive direction, reaches the maximum quickly, i.e., not far from position zero, and then stays for the rest of the trajectory in the narrow region between the small maximum and zero. This is very unlikely and becomes even more unlikely for $t_{\rm l}$ approaching $t_{\rm m}$. Therefore $P_{13}(t_{\rm l}, t_{\rm m}|t) \to 0$ vanishes rapidly as $t_{\rm l}$ approaches $t_{\rm m}$ from below. On the other hand, for $t_{\rm l} \to t_{\rm m}$ from above, the last passage is almost sure downward to the negative part, thus there are many trajectories possible, which leads to a much higher probability, explaining the jump in $P_{13}(t_{\rm l}, t_{\rm m}|t)$ as a function of $t_{\rm l}$. This property may hold for other types of stochastic processes as well. In Appendix C, we also analyze the magnitude of this discontinuity as a function of $t_{\rm m}$.

IV. CONCLUSIONS

We have computed analytically, and verified numerically, the pairwise joint distributions for three global quantities $t_{\rm o}$ (occupation time), $t_{\rm m}$ (time of the maximum) and $t_{\rm l}$ (last-passage time) for a one-dimensional Brownian time series of duration t. The main conclusion is that while the marginal distributions of these three variables all follow the same arcsine law, their joint distributions display very nontrivial and rich behaviors. Of the three pairs, some exhibit positive correlation while others weak anticorrelations. For example, $t_{\rm o}$ and $t_{\rm m}$ exhibit positive correlations, while $t_{\rm o}$ and $t_{\rm l}$ display weak higher order anticorrelations. Such behaviors could not have been guessed without the explicit exact results obtained in this paper. An interesting open problem is to compute explicitly the correlations between $t_{\rm l}$ and $t_{\rm m}$. Ironically for this pair, it seems easier to obtain the full joint distribution as presented in the paper rather than the moments of this distribution.

To the best of our knowledge, these interesting questions about correlations between global observables have never been addressed in the literature for any stochastic process, even though they seem natural enough. Since Brownian motion is the simplest, and yet the most ubiquitous stochastic process appearing in many areas from physics to biology, our results may thus serve as a future benchmark in many applications. In addition, it would be interesting to address these questions for other processes, e.g., a natural one being the Ornstein-Uhlenbeck (OU) process in one dimension. The OU process corresponds to a overdamped Brownian particle diffusing in the presence of a harmonic potential. Unlike the Brownian motion, the OU process is a stationary process. For such stationary processes, the occupation time distribution does not exhibit the arcsine law as in Brownian motion, but rather a large-deviation behavior [52], i.e., in the limit $t_{\rm o}$ large, t large but with their ration $t_{\rm o}/t$ fixed, one gets

$$p_{\rm o}(t_{\rm o}|t) \sim \exp\left[-t\,\Phi\left(\frac{t_{\rm o}}{t}\right)\right] \qquad (13)$$

where the rate function $\Phi(z)$ can be computed for the OU process [108]. Similarly, the marginal distribution $p_{\rm m}(t_m|t)$ also exhibits quite different behavior compared to the arcsine laws [70, 75]. It would certainly be interesting to compute joint distributions of these three observables for the OU process.

Finally, since joint distributions carry much more information about a system than the marginal distributions, obtaining them for other stochastic processes will be of high general interest. In particular this will also allow for practical applications to investigate hidden properties by exploiting the knowledge of correlations, e.g., between two quantities where one is easily accessible, while the other is not.

ACKNOWLEDGMENTS

SNM acknowledges the Alexander von Humboldt foundation for the Gay Lussac-Humboldt prize that allowed a visit to the Physics department at Oldenburg University, Germany where most of this work was performed. The simulations were performed at the the HPC cluster ROSA, located at the University of Oldenburg (Germany) and funded by the DFG through its Major Research Instrumentation Program (INST 184/225-1 FUGG) and the Ministry of Science and Culture (MWK) of the Lower Saxony State.

Appendix A: Joint distribution of the last-passage time t_l and the occupation time t_o for a Brownian motion of duration t

We consider the Brownian motion $x(\tau)$ of total duration t, starting at $x(0) = 0$. In this section we compute the joint distribution $P_{12}(t_l, t_o|t)$ of the last-passage time t_l and the occupation time t_o for fixed t. The process crosses the origin for the last time before t at the instant $\tau = t_l$ (see Fig. (6)).

Here we compute exactly the joint distribution $P_{12}(t_l, t_o|t)$ for a fixed total duration t. To proceed, we consider a typical trajectory of the Brownian motion as in Fig. (6). The idea is to first express the joint distribution as

$$P_{12}(t_l, t_o|t) = P_{\rm cond}(t_o|t_l|t)\, p_1(t_l|t)\,, \tag{A1}$$

where $P_{\rm cond}(t_o|t_l|t)$ denotes the conditional distribution of t_o given t_l and t, while $p_1(t_l|t)$ is the marginal distribution of t_l following the arcsine law. To compute the conditional probability $P_{\rm cond}(t_o|t_l|t)$, given t_l and t, we split the total duration t into two intervals (see Fig. (6)): (I) $0 \le \tau \le t_l$ and (II) $t_l \le \tau \le t$. Consequently, t_o can also be split into two parts

$$t_o = t_o^{\rm I} + t_o^{\rm II}\,, \tag{A2}$$

where the two random variables $t_o^{\rm I}$ and $t_o^{\rm II}$ are independent of each other, for a given fixed t_l. The idea then would be to compute the probability distribution function (PDF) of each of them separately and then convolute them to compute the full conditional probability. Below we compute the PDF's of $t_o^{\rm I}$ and $t_o^{\rm II}$ separately.

Interval I ($0 \le \tau \le t_l$). In this interval the Brownian motion starts at the origin at $\tau = 0$ and ends at the origin at $\tau = t_l$. Thus we have a Brownian bridge of duration t_l and we want to compute the PDF of $t_o^{\rm I} = \int_0^{t_l} \theta(x(\tau))\, d\tau$. It is well known that for a bridge of duration t_l, the PDF of the occupation time $t_o^{\rm I}$ is flat [103], i.e.,

$$p_{\rm I}(t_o^{\rm I}|t_l) = \frac{1}{t_l}\,\theta\left(t_l - t_o^{\rm I}\right)\,. \tag{A3}$$

The theta function gurantees that $t_o^I \le t_l$. One can also derive this result using the Feynman-Kac equation (by easily adapting the method described in e.g. Ref. [104] for a free Brownian motion). For convenience, we add a short derivation of this result later in the last section of this Supplemental Material.

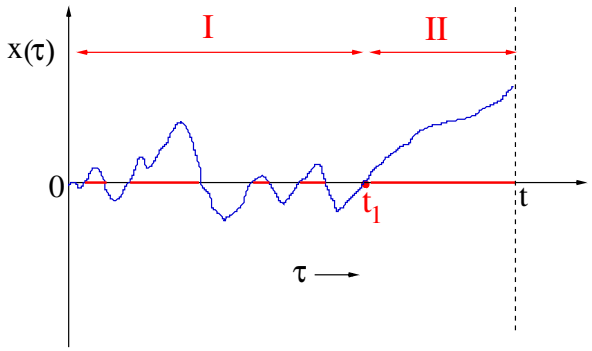

FIG. 6. A typical trajectory of a 1-d Brownian motion $x(\tau)$ of total duration t, starting at the origin $x(0) = 0$ and passing the origin for the last time before t at $\tau = t_l$. Solid red lines show the intervals during which $x(\tau)$ stays positive. The interval $[0, t_l]$ and $[t_l, t]$ are marked respectively I and II.

Interval II ($0 \le \tau \le t_l$). We first note that when the process crosses zero for the last time at $\tau = t_l$ (see Fig. (6)), it may do so either from above or below with equal probability $1/2$. If it crosses zero from above, then for the interval II, i.e., for $\tau \in [t_l, t]$, the process stays below zero indicating $t_o^{\rm II} = 0$. In contrast, if it crosses from zero from below at $\tau = t_l$ for the last time, it stays above zero in interval II, indicating $t_o^{\rm II} = (t - t_l)$. Since the two events occur with equal probability $1/2$, the distribution of the occupation time for the interval II is simply given by

$$p_{\rm II}(t_o^{\rm II}|t_l) = \frac{1}{2}\,\delta\left(t_o^{\rm II}\right) + \frac{1}{2}\,\delta\left(t_o^{\rm II} - (t - t_l)\right)\,. \tag{A4}$$

Since the total occupation time $t_o = t_o^{\rm I} + t_o^{\rm II}$ in Eq. (A2) is the sum of these two independent variables $t_o^{\rm I}$ and $t_o^{\rm II}$ (for fixed given t_l), its conditional distribution is given by the convolution

$$P_{\rm cond}(t_o|t_l|t) = \int_0^t dt_o^{\rm I}\, p_{\rm I}(t_o^{\rm I})\, p_{\rm II}(t_o - t_o^{\rm I})\,. \tag{A5}$$

Substituting the results from Eqs. (A3) and (A4) in Eq. (A5) gives (after carefully taking into acount when the delta functions contribute to the integral)

$$P_{\rm cond}(t_o|t_l|t) = \left[\frac{1}{2\,t_l}\,\theta(t_l - t_o) + \frac{1}{2\,t_l}\,\theta(t_o - (t - t_l))\right]\,\theta(t - t_o)\,. \tag{A6}$$

One can easily verify the normalization

$$\int_0^t P_{\rm cond}(t_o|t_l|t)\, dt_o = 1\,. \tag{A7}$$

We now substitute the result from Eq. (A6) into Eq. (A1) and use the arcsine result for the marginal distribution of t_l.

This gives our final result for the joint distribution of t_1 and t_o

$$P_{12}(t_1,t_o|t) = \frac{[\theta(t_1-t_o)+\theta(t_o-(t-t_1))]\;\theta(t-t_o)\,\theta(t-t_1)}{2\,\pi\,t_1^{3/2}\,\sqrt{t-t_1}}\,. \quad \text{(A8)}$$

It is convenient to express this joint PDF in the scaling form

$$P_{12}(t_1,t_o|t) = \frac{1}{t^2}\,\mathcal{P}_{12}\left(\frac{t_1}{t}=x,\,\frac{t_o}{t}=y\right)\,, \quad \text{(A9)}$$

where the scaling function $\mathcal{P}_{12}(x,y)$ for $0\le x\le 1$ and $0\le y\le 1$ is given by (8). One can check that the scaling function is normalized to unity

$$\int_0^1\int_0^1 dx\,dy\,\mathcal{P}_{12}(x,y) = 1\,. \quad \text{(A10)}$$

Furthermore, integrating over y only or x only, one recovers the marginal arcsine-law distributions, respectively. Finally, we note that as in the case of marginal distributions, the joint distribution of t_1 and t_o is also independent of the diffusion constant D of the Brownian motion.

To visualize this scaled joint PDF (8) in the (x,y) plane (actually in the square $[0,1]\times[0,1]$), it is useful to fix y and observe the scaled joint PDF as a function of x (along a horizontal slice in the (x,y) plane). There are two situations $0\le y\le 1/2$ and and $1/2<y\le 1$ that we consider separately.

Case 1: $0\le y\le 1/2$. In this case, since $y\le 1/2$, it is clear that $y\le 1-y$. We then have three regions as a function of x, for fixed $0\le y\le 1/2$, where the scaled joint PDF in Eq. (8) takes the following form

$$\mathcal{P}_{12}(x,y) = \begin{cases} 0\,, & \text{for}\quad 0\le x<y\,,\\ \frac{1}{2\,\pi\,x^{3/2}\,\sqrt{1-x}}\,, & \text{for}\quad y<x<1-y\\ \frac{1}{\pi\,x^{3/2}\,\sqrt{1-x}}\,, & \text{for}\quad 1-y<x\le 1\,. \end{cases} \quad \text{(A11)}$$

Thus the scaled joint PDF, as a function of x for fixed $0\le y\le 1/2$, undergoes two discontinuous jumps as a function of x, respectively at $x=y$ and $x=1-y$.

Case 2: $1/2\le y\le 1$. In this case, the scaling function in Eq. (8) reads

$$\mathcal{P}_{12}(x,y) = \begin{cases} 0\,, & \text{for}\quad 0\le x<1-y\,,\\ \frac{1}{2\,\pi\,x^{3/2}\,\sqrt{1-x}}\,, & \text{for}\quad 1-y<x<y\\ \frac{1}{\pi\,x^{3/2}\,\sqrt{1-x}}\,, & \text{for}\quad y<x\le 1\,. \end{cases} \quad \text{(A12)}$$

Here again, for fixed y, as a function of x, the scaling function undergoes discontinuous jumps at $x=1-y$ and $x=y$.

Combining these two behaviors for $y\le 1/2$ and $y\ge 1/2$, we obtain 4 distinct triangular regimes in the 2-d $(x-y)$ square of unit length, that are separated by the two diagonal lines $y=x$ and $y=1-x$. In the triangle $(x<y<1-x)\times(x<1/2)$, we have $\mathcal{P}_{12}(x,y)=0$. In the triangles $(y<x<1-y)\times(y<1/2)$ and $(1-y<x<y)\times(y>1/2)$, we have $\mathcal{P}_{12}(x,y)=1/[2\,\pi\,x^{3/2}\,\sqrt{1-x}]$. Finally, in the triangle $(1-x<y<x)\times(x>1/2)$, we have $\mathcal{P}_{12}(x,y)=1/[\pi\,x^{3/2}\,\sqrt{1-x}]$.

Correlation between t_1 and t_o. Given the joint distribution function in Eq. (8) one can compute the joint moments of the form

$$\langle t_1^m\,t_o^n\rangle = t^2\,\langle x^n\,y^n\rangle = t^2\,\int_0^1 dx\int_0^1 dy\,x^m\,y^n\,\mathcal{P}_{12}(x,y) \quad \text{(A13)}$$

Interestingly, even though the joint distribution (8) does not factorise, the explicit calculation of the covariance shows that it vanishes

$$\langle x\,y\rangle - \langle x\rangle\,\langle y\rangle = 0\,. \quad \text{(A14)}$$

It also turns out that

$$\langle x^2\,y\rangle - \langle x^2\rangle\,\langle y\rangle = 0\,, \quad \text{(A15)}$$

which raises the possibility that maybe there is a hidden factorisation of $\mathcal{P}_{12}(x,y)$ into a product of a function of x and a function of y. To test this, we computed the correlator

$$\langle x\,y^2\rangle - \langle x\rangle\,\langle y^2\rangle = -\frac{1}{48}\,, \quad \text{(A16)}$$

which clearly is nonzero, thus ruling out the factorisation. We further computed

$$\langle x^2\,y^2\rangle - \langle x^2\rangle\,\langle y^2\rangle = -\frac{7}{384}\,, \quad \text{(A17)}$$

exhibiting again a nonzero correlation. Thus clearly the correlations become nonzero only at higher orders. Moreover, the negative sign indicates that t_1 and t_o are weakly anti-correlated.

We have verified these analytical predictions numerically to very high precision in direct Monte Carlo data. We have performed simulations consisting of 10^8 independent simulations for $n_t=1000$ and $n_t=10000$ steps, respectively with step size $\Delta t=1$. We obtained for (A16) a value of $-0.0209(1)$, where the error bar reflects the difference between the two results for the two values of n_s. This compares well with $-1/48\approx -0.02083$. For (A17) we obtained 0.01820(3), compared to $-7/384\approx -0.01823$.

Appendix B: Joint distribution of the occupation time t_o and the time t_m of the maximum for a Brownian motion of duration t

In this section, our goal is to compute the joint distribution $P_{23}(t_o,t_m|t)$ of the random variables t_o and t_m, given the fixed total duration t. Here our result is less explicit. Let

us summarize our main result. We first define the following triple Laplace transform of the joint distribution $P_{23}(t_{\rm o},\, t_{\rm m}|t)$ as

$$\int_0^\infty dt\, e^{-s\,t} \int_0^t dt_{\rm o}\, e^{-p\,t_{\rm o}} \int_0^t dt_{\rm m}\, e^{-\lambda\, t_{\rm m}} P_{23}(t_{\rm o},\, t_{\rm m}|t) = \int_0^\infty dt\, e^{-s\,t} \left\langle e^{-p\,t_{\rm o}-\lambda\, t_{\rm m}} \right\rangle . \quad \text{(B1)}$$

For this quantity, we find the following exact result

$$\int_0^\infty dt\, e^{-s\,t} \left\langle e^{-p\,t_{\rm o}-\lambda\, t_{\rm m}} \right\rangle = \frac{1}{(s+p)} \int_0^\infty dx\, \frac{\left[\sinh(x) + \sqrt{\frac{s}{s+p}}\, \cosh(x) + \frac{p}{s}\sqrt{\frac{s}{s+p}}\right]}{\left[\cosh(x) + \sqrt{\frac{s}{s+p}}\, \sinh(x)\right] \left[\sqrt{\frac{s+\lambda}{s+p+\lambda}}\, \sinh\left(\sqrt{\frac{s+p+\lambda}{s+p}}\, x\right) + \cosh\left(\sqrt{\frac{s+p+\lambda}{s+p}}\, x\right)\right]} . \quad \text{(B2)}$$

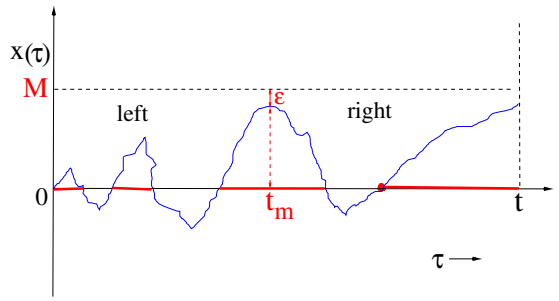

FIG. 7. A typical trajectory of a 1-d Brownian motion $x(\tau)$ of total duration t, starting at the origin $x(0) = 0$ and achieving it maximum value $M - \epsilon$ at time $t_{\rm m}$. Solid red lines show the intervals during which $x(\tau)$ stays positive. The interval $[0, t_{\rm m}]$ and $[t_{\rm m}, t]$ are marked respectively left and right. Both on the left and right regions, the trajectory stays below the level M, since by definition M is the maximum. The cut-off ϵ is introduced for the convenience of calculation and eventually we take the limit $\epsilon \to 0$.

Even though it is hard to invert this triple Laplace tarnsform to extract the joint distribution $P_{23}(t_{\rm o}, t_{\rm m}|t)$ explicitly, the result in Eq. (B2) gives us access to exact moments and correlation functions as shown below. The derivation of this principal result in Eq. (B2) is somewhat involved. We will just outline below the main steps and the readers not interested in the derivation may skip this part and move directly to the explicit results on moments and correlation functions derived later from this formula.

To compute the joint distribution $P_{23}(t_{\rm o}, t_{\rm m}|t)$, we generalise a path-decomposition method that was originally used in Ref. [27] to compute the joint distribution of the global maximum M and the time $t_{\rm m}$ at which it occurs for a Brownian motion of duration t. The idea is to first compute an extended joint distribution $P(t_{\rm o}, t_{\rm m}, M|t)$ of the three random variables $t_{\rm o}$, $t_{\rm m}$ and the value of the maximum M and then integrate over M to obtain the joint distribution of $t_{\rm o}$ and $t_{\rm m}$

$$P_{23}(t_{\rm o}, t_{\rm m}|t) = \int_0^\infty P(t_0, t_{\rm m}, M|t)\, dM\, . \quad \text{(B3)}$$

The computation of $P(t_0, t_{\rm m}, M|t)$ can be performed using a path decomposition method that exploits the Markov property of the process and is best understood by following a trajectory as depicted in Fig. (7). We first divide the full interval $[0, t]$ into two parts: (i) 'left' part over $[0, t_{\rm m}]$ and (ii) 'right' part over $[t_{\rm m}, t]$. In the left part, the trajectory $x(\tau)$, starting at 0, has to remain below M till time $t_{\rm m}$ and it arrives at its maximal value M exactly at the instant $t_{\rm m}$. On the right side, the process, starting at M exactly at $t_{\rm m}$ needs to stay below M till time t. Normally, the constraint of staying below M can be imposed by putting an absorbing boundary at the level M. However, imposing an absorbing boundary at $x = M$ during $[0, t]$ also forbids the process to reach exactly at M at time $t_{\rm m}$. To satisfy both constraints, i.e., staying below M during the full interval $[0, t]$ and at the same time arriving at M at the instant $t = t_{\rm m}$, one can use the trick of putting a small cut-off ϵ and imposing the condition that the process reaches $M - \epsilon$ at $t = t_{\rm m}$, while staying below M through out the interval $[0, t]$. Then there is no problem in imposing an absorbing boundary condition at $x = M$ during the full interval $[0, t]$. Finally, we will take the limit $\epsilon \to 0$ in an appropriate way at the very end of the calculation. This limiting procedure using an ϵ cut-off has been successfully used in many examples of computing observables for constrained Brownian motions [27, 70, 75, 81, 98, 99, 105–107], and we will henceforth call it the ϵ-path decomposition method.

In the current problem, in addition to $t_{\rm m}$ and M, we need also to keep track of the occupation time $t_{\rm o}$. Let us also divide it into two parts, one from the left of $t_{\rm m}$ and one from the right

of $t_{\rm m}$, i.e.,

$$t_{\rm o} = \int_0^t \theta\left(x(\tau)\right)\, d\tau = \int_0^{t_{\rm m}} \theta\left(x(\tau)\right)\, d\tau + \int_{t_{\rm m}}^t \theta\left(x(\tau)\right)\, d\tau = t_{\rm o}^{\rm L} + t_{\rm o}^{\rm R}\,, \quad \text{(B4)}$$

where the superscripts L and R refer respectively to the left and right of $t_{\rm m}$. For the left part, let $G_M(M-\epsilon, t_{\rm m}, t_{\rm o}^{\rm L}|0,0)$ denote the restricted propagator of the Brownian motion from the position 0 at time 0 to position $M-\epsilon$ at time $t_{\rm m}$ and carrying an occupation time $t_{\rm o}^{\rm L}$, in the presence an absorbing boundary at $x = M$ (see Fig (7)). Similarly, for the right part, let $Q_M(M-\epsilon, t-t_{\rm m}, t_{\rm o}^{\rm R})$ denote the probability that the process, starting at $M-\epsilon$ at time $t_{\rm m}$ will stay below the level M up to time t and will carry an occupation time $t_{\rm o}^R$ (see Fig. (7)). Then using the Markov property of the process, we have

$$P(t_{\rm o}, t_{\rm m}, M|t) = \mathcal{N}(\epsilon)\times \int_0^{t_{\rm o}} dt_{\rm o}^{\rm L}\, G_M(M-\epsilon, t_{\rm m}, t_{\rm o}^{\rm L}|0,0)\, Q_M(M-\epsilon, t-t_{\rm m}, t_{\rm o}-t_{\rm o}^{\rm L})\,, \quad \text{(B5)}$$

where we used the decomposition in Eq. (B4). We have introduced a proportionality constant $\mathcal{N}(\epsilon)$ which will be fixed later from the normalization of the joint probability density, once we take the $\epsilon \to 0$ limit at the end of the calculation. Due to the convolution structure of the right hand side (rhs) of Eq. (B5) with respect to both $t_{\rm o}$ and $t_{\rm m}$, it is then natural to define a Laplace transform with respect to all three variables $t_{\rm o}$, $t_{\rm m}$ and t

$$\tilde{P}(M,p,\lambda,s) = \int_0^\infty dt\, e^{-s\,t} \int_0^t dt_{\rm o}\, e^{-p\,t_{\rm o}} \int_0^t dt_{\rm m}\, e^{-\lambda\, t_{\rm m}}\, P(t_{\rm o}, t_{\rm m}, M|t)\,. \quad \text{(B6)}$$

Taking this triple Laplace transform in Eq. (B5) gives

$$\tilde{P}(M,p,\lambda,s) = \mathcal{N}(\epsilon)\, \tilde{G}_M(M-\epsilon, \lambda+s, p)\, \tilde{Q}_M(M-\epsilon, s, p)\,. \quad \text{(B7)}$$

Here we have defined

$$\tilde{G}_M(x,s,p) = \int_0^\infty dT e^{-s\,T} \int_0^t dt_{\rm o}\, e^{-p\,t_{\rm o}}\, G_M(x, T, t_{\rm o}|0,0), \quad \text{(B8)}$$

where $G_M(x,T,t_{\rm o}|0,0)$ (with $x < M$) is simply the propagator of a Brownian motion from $(0,0)$ to (x,T) with occupation time $t_{\rm o}$ in $[0,T]$ and in the presence of an absorbing boundary at $x = M$. Similarly

$$\tilde{Q}_M(x_0,s,p) = \int_0^\infty dT\, e^{-s\,T} \int_0^t dt_{\rm o}\, e^{-p\,t_{\rm o}}\, Q_M(x_0, T, t_{\rm o})\,, \quad \text{(B9)}$$

where $Q_M(x_0, t_{\rm o}, T)$ is the probability that a Brownian path, starting at $x_0 < M$ at time 0, stays below M up to time T and carries an occupation time $t_{\rm o}$ in $[0,T]$.

Thus we need two auxiliary ingredients, namely the two restricted propagators $\tilde{G}_M(x,s,p)$ and $\tilde{Q}_M(x_0,s,p)$, in order to compute the rhs of Eq. (B7). Fortunately, these two restricted propagators (rather their Laplace transforms) can be computed using the Feynman-Kac formalism. For example, consider first $G_M(x,T,t_{\rm o}|0,0)$ (with $x < M$) and define its Laplace transform with respect to $t_{\rm o}$ only, i.e.,

$$\tilde{g}_M(x,T,p) = \int_0^T dt_{\rm o}\, e^{-p\,t_{\rm o}}\, G_M(x,T,t_{\rm o}|0,0)\,. \quad \text{(B10)}$$

From the definition $t_{\rm o} = \int_0^T \theta\left(x(\tau)\right)\, d\tau$, we thus have a functional of Brownian motion and consequently $\tilde{g}_M(x,T,p)$ satisfies the Feynman-Kac equation

$$\partial_T \tilde{g}_M(x,T,p) = D\,\partial_x^2 \tilde{g}_M(x,T,p) - p\,\theta(x)\,\tilde{g}_M(x,T,p)\,, \quad \text{(B11)}$$

valid for $x \le M$ with the absorbing boundary condition $\tilde{g}_M(x=M,T,p) = 0$. The initial condition reads $\tilde{g}_M(x, T=0, p) = \delta(x)$, since the process starts at the origin. Next we take a Laplace transform with respect to T and define

$$\tilde{G}_M(x,s,p) = \int_0^\infty dT\, e^{-s\,T}\, \tilde{g}_M(x,T,p)\,. \quad \text{(B12)}$$

Taking Laplace transform of Eq. (B11) with respect to T and using the initial condition gives us an ordinary second order differential equation for $\tilde{G}_M(x,s,p)$

$$D\,\frac{d^2\tilde{G}_M(x,s,p)}{dx^2} - \left[p\,\theta(x) + s\right]\,\tilde{G}_M(x,s,p) = -\delta(x) \quad \text{(B13)}$$

for $x \le M$, with the boundary conditions $\tilde{G}_M(x = M, s, p) = 0$ and $\tilde{G}_M(x \to -\infty, s, p) = 0$. The differential equation can be solved exactly (in two regions $0 \le x \le M$ and $x \le 0$ and then by matching the two solutions at $x = 0$). Omitting details, we get

$$\tilde{G}_M(x,s,p) = \frac{\sinh\left(\sqrt{\frac{s+p}{D}}\,(M-x)\right)}{\sqrt{D}\left[\sqrt{s}\,\sinh\left(\sqrt{\frac{s+p}{D}}\,M\right) + \sqrt{s+p}\,\cosh\left(\sqrt{\frac{s+p}{D}}\,M\right)\right]}\,. \quad \text{(B14)}$$

Now setting $x = M - \epsilon$ and taking $\epsilon \to 0$ limit, we obtain to leading order in ϵ

$$\tilde{G}_M(M-\epsilon,s,p) = \frac{\sqrt{s+p}}{D\left[\sqrt{s}\,\sinh\left(\sqrt{\frac{s+p}{D}}\,M\right) + \sqrt{s+p}\,\cosh\left(\sqrt{\frac{s+p}{D}}\,M\right)\right]}\,\epsilon \quad \text{(B15)}$$

plus Terms of order $O(\epsilon^2)$. Finally, replacing s by $\lambda + s$ as required in Eq. (B7), we get for the left half (of $t_{\rm m}$) the propagator (up to order ϵ)

$$\tilde{G}_M(M-\epsilon,\lambda+s,p) \approx \frac{\sqrt{s+\lambda+p}}{D\left[\sqrt{\lambda+s}\,\sinh\left(\sqrt{\frac{\lambda+s+p}{D}}\,M\right)+\sqrt{\lambda+s+p}\,\cosh\left(\sqrt{\frac{\lambda+s+p}{D}}\,M\right)\right]}\,\epsilon\,. \tag{B16}$$

We now turn to the right part of $t_{\rm m}$. Here we again define first the Laplace transform of $Q_M(x_0,t_{\rm o},T)$ with respect to $t_{\rm o}$ only

$$\tilde{q}(x_0,T,p)=\int_0^T dt_{\rm o}\,e^{-p\,t_{\rm o}}\,Q_M(x_0,T,t_{\rm o})\,. \tag{B17}$$

Then, $\tilde{q}(x_0,T,p)$ satisfies the backward Feynman-Kac equation (where one treats the starting position x_0 as the variable [104])

$$\partial_T\tilde{q}_M(x_0,T,p)=D\,\partial^2_{x_0}\tilde{q}_M(x_0,T,p)-p\,\theta(x_0)\,\tilde{q}_M(x_0,T,p)\,, \tag{B18}$$

valid for $x_0\le M$ with an absorbing boundary condition $\tilde{q}_M(x_0=M,T,p)=0$. The initial condition is $\tilde{q}_M(x_0,T=0,p)=1$ for all $x_0<M$. Taking again Laplace transform with respect to T reduces the partial differential equation to an ordinary second order differential equation for $\tilde{Q}_M(x_0,s,p)=\int_0^\infty dT\,e^{-s\,T}\,\tilde{q}_M(x_0,T,p)$, leading to

$$D\,\frac{d^2\tilde{Q}_M(x_0,s,p)}{dx_0^2}-[p\,\theta(x_0)+s]\;\tilde{Q}_M(x_0,s,p)=-1 \tag{B19}$$

for $x\le M$. Once again, one can solve this differential equation explicitly, with a long and ugly (but explicit) solution. However, if one now sets $x_0=M-\epsilon$ as required in Eq. (B7) and expands for small ϵ, one gets a relatively simpler expression for the leading order in ϵ

$$\tilde{Q}_M(m-\epsilon,s,p)\approx\frac{\epsilon}{\sqrt{D\,(s+p)}}\,\frac{\left[\sinh\left(\sqrt{\frac{s+p}{D}}\,M\right)+\sqrt{\frac{s}{s+p}}\,\cosh\left(\sqrt{\frac{s+p}{D}}\,M\right)+\frac{p}{\sqrt{s(s+p}}\right]}{\left[\cosh\left(\sqrt{\frac{s+p}{D}}\,M\right)+\sqrt{\frac{s}{s+p}}\,\sinh\left(\sqrt{\frac{s+p}{D}}\,M\right)\right]}\,. \tag{B20}$$

Finally, substituting the results from Eq. (B16) and (B20) into Eq. (B7) and taking the limit $\epsilon\to 0$ gives

$$\tilde{P}(M,p,\lambda,s)=\frac{A_1\,\left[\sinh\left(\sqrt{\frac{s+p}{D}}\,M\right)+\sqrt{\frac{s}{s+p}}\,\cosh\left(\sqrt{\frac{s+p}{D}}\,M\right)+\frac{p}{\sqrt{s\,(s+p)}}\right]}{\left[\sqrt{\frac{\lambda+s}{\lambda+s+p}}\,\sinh\left(\sqrt{\frac{\lambda+s+p}{D}}\,M\right)+\cosh\left(\sqrt{\frac{\lambda+s+p}{D}}\,M\right)\right]\,\left[\cosh\left(\sqrt{\frac{s+p}{D}}\,M\right)+\sqrt{\frac{s}{s+p}}\,\sinh\left(\sqrt{\frac{s+p}{D}}\,M\right)\right]}\,, \tag{B21}$$

where the constant A_1 is given by

$$A_1=\frac{1}{D\,\sqrt{D\,(s+p)}}\,\left[\lim_{\epsilon\to 0}\mathcal{N}(\epsilon)\,\epsilon^2\right]\,. \tag{B22}$$

One can check a posteriori that in order that $P(M,t_{\rm o},t_{\rm m}|t)$ is normalized to unity when intergrated over M, $t_{\rm m}$ and $t_{\rm o}$, we must have the identity

$$\lim_{\epsilon\to 0}\mathcal{N}(\epsilon)\,\epsilon^2=D\quad\text{ implying }\quad A_1=\frac{1}{\sqrt{D\,(s+p)}}\,. \tag{B23}$$

We use this result in Eq. (B21) and then integrate over M as in Eq. (B3), with the change of variable $M\sqrt{(s+p)/D}=x$. This then yields the final result announced in Eq. (B2), thus completing its derivation.

Marginals, moments and correlation functions: Our main result in this section, namely Eq. (B2), is exact but somewhat formal. We now show how to exploit this exact result (B2) on the triple Laplace transform to extract as much information as possible, which can then be checked numerically.

Marginals. As a first check, we consider the marginals. Setting $p=0$ in Eq. (B2) and carrying out the integral over x on the rhs of Eq. (B2) gives

$$\int_0^\infty dt\,e^{-st}\,\int_0^t dt_{\rm m}\,e^{-\lambda\,t_{\rm m}}\,P(t_{\rm m}|t)=\frac{1}{\sqrt{s\,(s+\lambda)}}\,, \tag{B24}$$

where $P(t_{\rm m}|t)=\text{Prob.}[t_{\rm m}|t]$ is the marginal distribution of $t_{\rm m}$ for fixed total duration t. To invert the double Laplace transform in Eq. (B24), we first write $t_1=t-t_{\rm m}$ and split $t=t_{\rm m}+t_1$. Then Eq. (B24) reduces to

$$\int_0^\infty dt_{\rm m}\,e^{-(s+\lambda)\,t_{\rm m}}\,\int_0^\infty dt_1\,e^{-s\,t_1}\,P(t_{\rm m}|t)=\frac{1}{\sqrt{s\,(s+\lambda)}}\,. \tag{B25}$$

Now, the inverse Laplace transform of $1/\sqrt{s}$ is simply given by $\mathcal{L}^{-1}_{s\to t_1}=1/\sqrt{\pi\,t_1}$. Using this we invert both Laplace transforms separately in Eq. (B25) we recover the well known arcsine law for the marginal distribution of $t_{\rm m}$

$$P(t_{\rm m}|t)=\frac{1}{\pi}\,\frac{1}{\sqrt{t_{\rm m}\,(t-t_{\rm m})}}\quad\text{ with }\quad 0\le t_{\rm m}\le t\,. \tag{B26}$$

Similarly, setting $\lambda = 0$ in Eq. (B2), one can again carry out the integral over x explicitly on the rhs of Eq. (B2), leading to

$$\int_0^\infty dt\, e^{-st} \int_0^t dt_{\rm o}\, e^{-p\, t_{\rm o}}\, P(t_{\rm o}|t) = \frac{1}{\sqrt{s\,(s+p)}}\,, \quad \text{(B27)}$$

where $P(t_{\rm o}|t) = {\rm Prob.}[t_{\rm o}|t]$ is the marginal distribution of $t_{\rm o}$ for fixed t. This double Laplace transform in Eq. (B27) can then be inverted using the same trick as in Eq. (B25) (just replacing λ by p) and thus one again recovers the arcsine law for the marginal distribution of $t_{\rm o}$

$$P(t_{\rm o}|t) = \frac{1}{\pi}\,\frac{1}{\sqrt{t_{\rm o}\,(t-t_{\rm o})}} \quad \text{with} \quad 0 \le t_{\rm o} \le t\,. \quad \text{(B28)}$$

The fact that we recover the correct normalized marginals also proves, a posteriori, the normalization condition in Eq. (B23).

Moments and correlation functions. For general p and λ, it is very hard to invert the triple Laplace transform in Eq. (B2) explicitly. However, we were able to extract various cross-moments by expanding both sides of Eq. (B2) in powers of p and λ and matching their coefficients. These coefficients are still functions of s and we were able to invert these Laplace transforms with respect to s explicitly. This can be systematically done using the Mathematica. This allowed us to compute various covariance functions explicitly. We quote here some examples.

$$\langle t_{\rm o}\, t_{\rm m}\rangle - \langle t_{\rm o}\rangle\, \langle t_{\rm m}\rangle \;=\; \frac{11}{144}\, t^2\,, \quad \text{(B29)}$$

$$\langle t_{\rm o}\, t_{\rm m}^2\rangle - \langle t_{\rm o}\rangle\, \langle t_{\rm m}^2\rangle \;=\; \frac{43}{648}\, t^3\,, \quad \text{(B30)}$$

$$\langle t_{\rm o}^2\, t_{\rm m}\rangle - \langle t_{\rm o}^2\rangle\, \langle t_{\rm m}\rangle \;=\; \frac{509}{7200}\, t^3\,, \quad \text{(B31)}$$

$$\langle t_{\rm o}^2\, t_{\rm m}^2\rangle - \langle t_{\rm o}^2\rangle\, \langle t_{\rm m}^2\rangle \;=\; \frac{25997}{414720}\, t^4\,. \quad \text{(B32)}$$

Thus the observables $t_{\rm o}$ and $t_{\rm m}$ are thus slightly positively correlated. We have verified these analytical predictions numerically, from the direct Monte Carlo data. We have performed simulations consisting of 10^8 independent simulations for $n_t = 1000$ and $n_t = 10000$ steps, respectively with step size $\Delta t = 1$. We obtained at $t = 1$, for (B29) a value of $0.0764(1)$, where the error bar reflects the difference between the two results for the two values of n_s. This compares well with $11/144 \approx 0.07639$. For (B30) we obtained 0.0664(1), compared to $43/648 \approx 0.06636$. For (B31) we obtained 0.0707(1), compared to $509/7200 \approx 0.07069$. For (B32) we obtained 0.0627(1), compared to $25997/414720 \approx 0.06269$.

Appendix C: Joint distribution of the last-passage time $t_{\rm l}$ and the time $t_{\rm m}$ of the maximum for a Brownian motion of duration t

In this section we compute the joint distribution $P_{13}(t_{\rm l}, t_m|t)$ of the two random variables $t_{\rm l}$ and $t_{\rm m}$, given the fixed total duration t. To compute this joint distribution via the ϵ-path decomposition method as in the previous section, it is convenient to introduce the enlarged joint distribution $P(t_{\rm l}, t_{\rm m}, M|t)$ of $t_{\rm l}$, $t_{\rm m}$ and the value M of the global maximum in $[0, t]$. Once we obtain this, one can integrate over M to obtain $P_{13}(t_{\rm l}, t_{\rm m}|t)$, i.e.,

$$P_{13}(t_{\rm l}, t_{\rm m}|t) = \int_0^\infty P(t_{\rm l}, t_{\rm m}, M|t)\, dM\,. \quad \text{(C1)}$$

To compute $P(t_{\rm l}, t_{\rm m}, M|t)$, we proceed as follows. It turns out that the results are quite different depending on whether $t_{\rm l} > t_{\rm m}$ or $t_{\rm l} < t_{\rm m}$. We start with the case $t_{\rm l} > t_{\rm m}$ and then proceed to $t_{\rm l} < t_{\rm m}$.

The case $t_{\rm l} > t_{\rm m}$. To compute $P(t_{\rm l}, t_{\rm m}, M|t)$ in this case, we again investigate a typical trajectory as shown in Fig. (8). Let M be the maximum of the Brownian motion of duration t that starts at the origin $x(0) = 0$. Let $t_{\rm m}$ and $t_{\rm l}$ denote respectively the time at which the maximum occurs and the last time the processes crosses 0 before t. For M to be the maximum, the process has to stay below M throughout which is implemented by an absorbing boundary condition for the trajectory at $x = M$. However, this forbids the process to arrive at M at time $t_{\rm m}$. Hence, as in the previous ssection, we put a cut-off ϵ_1 at $t = t_{\rm m}$ and impose that the process arrives at $M - \epsilon_1$ (with $\epsilon_1 \ge 0$) at time $t_{\rm m}$. Similarly, to impose the constraint that the process stays above or below the origin during $[t_{\rm l}, t_{\rm m}]$ we need to put an absorbing boundary condition at $x = 0$ which will again forbid the process to arrive at 0 exactly at $t_{\rm l}$. Hence, we need to introduce a second cut-off ϵ_2 at $t = t_{\rm l}$, i.e., impose that the process arrives at ϵ_2 at $t = t_{\rm l}$ and then does not cross zero during $[t_{\rm l}, t]$. Eventually, we will take the limits $\epsilon_1 \to 0$ and $\epsilon_2 \to 0$ in appropriate ways as in the previous section.

To proceed with the computation we then divide the full time interval $[0, t]$ into three subintervals (see Fig. (8)): (I) the interval $[0, t_{\rm m}]$ where the process, starting at the origin and staying below the level M, arrives at $M - \epsilon_1$ (II) starting at $M - \epsilon_1$ at time $t_{\rm m}$ the process arrives at $\epsilon_2 > 0$ at time $t_{\rm l}$, while staying below M and (III) starting at ϵ_2 the process stays below M and does not cross the origin during $[t_{\rm l}, t]$. For each of these intervals, we will compute the propagator of the path and then take their product to compute the full propagator satisfying all the constraints.

Interval I ($0 \le \tau \le t_{\rm m}$)**.** In this case, we have a Brownian path propagating from 0 at $\tau = 0$ to $x(t_{\rm m}) = M - \epsilon_1$ at time $\tau = t_{\rm m}$, but with the restriction that the path stays below M. Let $G(x, x_0, \tau|M)$ denotes the probability density of arriving at x at time τ, starting from x_0 at $\tau = 0$ and staying below M till time τ. Then this propagator $G(x, x_0, \tau|M)$ satisfies the diffusion equation

$$\frac{\partial G}{\partial t} = D\,\frac{\partial^2 G}{\partial x^2} \quad \text{(C2)}$$

in the region $x \le M$, with the absorbing boundary condition $G(x = M, x_0, \tau|M) = 0$ and the initial condition $G(x, x_0, \tau = 0|M) = \delta(x - x_0)$. The solution can be easily

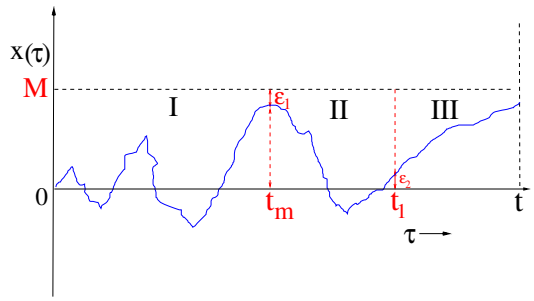

FIG. 8. A typical trajectory of a 1-d Brownian motion $x(\tau)$ of total duration t, starting at the origin $x(0) = 0$. The trajectory arrives at its maximum value $M - \epsilon_1$ at time $t_{\rm m}$ and arrives at ϵ_2 at time $t_{\rm l} > t_{\rm m}$ after which it does not cross the origin. We divide the total duration $[0, t]$ into three intervals: (I) the interval $[0, t_{\rm m}]$ where the process, starting at the origin and staying below the level M arrives at $M - \epsilon_1$ at time $t_{\rm m}$ (II) starting at $M - \epsilon_1$ at time $t_{\rm m}$ the process arrives at $\epsilon_2 > 0$ at time $t_{\rm l}$, while staying below M and (III) starting at ϵ_2 the process stays below M and does not cross the origin during $[t_{\rm l}, t]$. Eventually, we take the limits $\epsilon_1 \to 0$ and $\epsilon_2 \to 0$ at the end of the calculation.

found using the method of images [104] and it reads

$$G(x, x_0, \tau|M) = \frac{1}{\sqrt{4\,\pi\,D\,\tau}} \left[e^{-(x-x_0)^2/4D\tau} - e^{-(2M-x-x_0)^2/4D\tau} \right] . \quad \text{(C3)}$$

Setting $x = M - \epsilon_1$, $x_0 = 0$, $\tau = t_{\rm m}$ and expanding up to $O(\epsilon_1)$, we get the propagator G_I for part I

$$G_{\rm I} \approx \frac{\epsilon_1}{D} \frac{M}{\sqrt{4\,\pi\,D\,t_{\rm m}^3}}\, e^{-M^2/4Dt_{\rm m}} . \quad \text{(C4)}$$

Interval II ($t_{\rm m} \le \tau \le t_{\rm l}$)**.** In this second interval, the path starts at $M - \epsilon_1$ and reaches ϵ_2 at time $t_{\rm l}$, while staying below M during the trip. Hence, we can again use the general result in Eq. (C3) and set $x_0 = M - \epsilon_1$, $x = \epsilon_2$, $\tau = t_{\rm l} - t_{\rm m}$ to get the propagator $G_{\rm II}$ for the interval II. In addition, expanding in powers of ϵ_1 and ϵ_2, the leading nonzero term is given by

$$G_{\rm II} \approx \frac{\epsilon_1\,\epsilon_2}{D} \frac{M}{\sqrt{4\,\pi\,D\,(t_{\rm l} - t_{\rm m})^3}}\, e^{-M^2/4D(t_{\rm l}-t_{\rm m})} . \quad \text{(C5)}$$

Interval III ($t_{\rm l} \le \tau \le t$)**.** In this interval, the path propagates during the interval $\tau \in [t_{\rm l}, t]$, starting from ϵ_2 at $\tau = t_{\rm l}$, and does not cross zero during the interval $[t_{\rm l}, t]$. In addition, the path stays below the level M during $[t_{\rm l}, t]$. There are now two possibilities: (a) $\epsilon_2 > 0$, in which case the process stays positive during $[t_{\rm l}, t]$ and (b) $\epsilon_2 < 0$, in which case the path stays negative during $[t_{\rm l}, t]$. Let us first consider the case (a) where $\epsilon_2 > 0$ and the path stays inside the box $[0, M]$ during $[t_{\rm l}, t]$, starting at $\epsilon_2 > 0$ at the begining of the interval. Let us then consider the Brownian propagator $G_{\rm box}(x, x_0, T|M)$ as the probability density for a Brownian path to arrive at $0 \le x \le M$ at time T, starting from $0 \le x_0 \le M$ at $T = 0$, while staying inside the box $[0, M]$ during T. This propagator again satisfies the diffusion equation in $0 \le x \le M$

$$\frac{\partial G_{\rm box}}{\partial T} = D\, \frac{\partial^2 G_{\rm box}}{\partial x^2} \quad \text{(C6)}$$

with absorbing boundary conditions: $G_{\rm box}(x = M, x_0, T|M) = G_{\rm box}(x = 0, x_0, T|M) = 0$. The exact solution can be easily found and it reads

$$G_{\rm box}(x, x_0, T|M) = \frac{2}{M} \sum_{n=1}^{\infty} \sin\left(\frac{n\pi x}{M}\right) \sin\left(\frac{n\pi x_0}{M}\right) e^{-n^2\pi^2 DT/M^2} . \quad \text{(C7)}$$

Integrating over the final position gives the survival probability up to time T, starting at x_0,

$$S(x_0, T|M) = \frac{4}{\pi} \sum_{m=0}^{\infty} \frac{1}{2m+1} \sin\left(\frac{(2m+1)\pi x_0}{M}\right) e^{-(2m+1)^2\pi^2 DT/M^2} . \quad \text{(C8)}$$

Setting $T = t - t_{\rm l}$, $x_0 = \epsilon_2$ in Eq. (C8) and subsequently taking the limit $\epsilon_2 \to 0$ then gives the propagator for the interval III in the case (a) when $\epsilon_2 > 0$. We get, to leading order in ϵ_2,

$$G_{\rm III}^{(a)} \approx \frac{4\epsilon_2\,\theta(\epsilon_2)}{M} \sum_{m=0}^{\infty} e^{-(2m+1)^2\pi^2 D(t-t_{\rm l})/M^2} . \quad \text{(C9)}$$

Next we consider the case (b) where $\epsilon_2 < 0$. In this case, the walk starting at $\epsilon_2 < 0$, stays negative during $[t_{\rm l}, t]$ (the fact that it stays negative automatically guarantees that it stays below the level M since $M \ge 0$). The probability density $G_-(x, x_0, T)$ for a Brownian motion to reach $x < 0$, starting at $x_0 < 0$, and staying below 0 during an interval T, can again be computed by the method of images and is given simply by [104]

$$G_-(x, x_0, T) = \frac{1}{\sqrt{4\,\pi\,D\,T}} \left[e^{-(x-x_0)^2/4DT} - e^{-(x+x_0)^2/4DT} \right] . \quad \text{(C10)}$$

Integrating over $x \le 0$ gives the survival probability

$$S_-(x_0, T) = \mathrm{erf}\left(\frac{|x_0|}{\sqrt{4\,D\,T}}\right) \quad \text{where} \quad \mathrm{erf}(z) = \frac{2}{\sqrt{\pi}} \int_0^z e^{-u^2}\, du . \quad \text{(C11)}$$

Hence, setting $x_0 = \epsilon_2 < 0$, $T = t - t_{\rm l}$ and expanding to leading order in ϵ_2 then gives the propagator for interval III for the case (b) where $\epsilon_2 < 0$

$$G_{\rm III}^{(b)} \approx \frac{\epsilon_2\,\theta(-\epsilon_2)}{\sqrt{\pi\,D\,(t - t_{\rm l})}} . \quad \text{(C12)}$$

Finally, combining the two results in Eqs. (C9) for $\epsilon_2 > 0$ and (C12) for $\epsilon_2 < 0$, we get

$$G_{\rm III} \approx |\epsilon_2| \left[\frac{4}{M} \sum_{m=0}^{\infty} e^{-(2m+1)^2\pi^2 D(t-t_{\rm l})/M^2} + \frac{1}{\sqrt{\pi\, D\,(t-t_{\rm l})}} \right] . \tag{C13}$$

It is sometimes convenient to express the sum in Eq. (C13) slightly differently using the following Poisson summation formula

$$\sum_{m=0}^{\infty} e^{-\frac{(2m+1)^2\pi^2}{4z}} = \sqrt{\frac{z}{4\pi}} \left[1 + 2 \sum_{n=1}^{\infty} (-1)^n e^{-n^2 z} \right] \tag{C14}$$

for $z > 0$. Using this formula in Eq. (C13) gives us a more compact formula

$$G_{\rm III} \approx \frac{2\,|\epsilon_2|}{\sqrt{\pi\, D\,(t-t_{\rm l})}} \sum_{n=0}^{\infty} (-1)^n\, e^{-\frac{n^2 M^2}{4\,D\,(t-t_{\rm l})}} . \tag{C15}$$

Now that we have the required propagators for all the three intervals I, II and III respectively in Eqs. (C4), (C5) and (C15), we take their product using the Markov property of the process and obtain the joint distribution $P(t_{\rm l}, t_{\rm m}, M|t)$ for $t_{\rm l} > t_{\rm m}$ as

$$P(t_{\rm l}, t_{\rm m}, M|t) = \left[\lim_{\epsilon_1 \to 0} \mathcal{N}_1(\epsilon_1) \frac{\epsilon_1^2}{D} \right] \left[\lim_{\epsilon_2 \to 0} \mathcal{N}_2(\epsilon_2) \frac{\epsilon_2^2}{D} \right] \frac{\theta(t_{\rm l} - t_{\rm m})\, M^2}{2\,(\pi\, D)^{3/2}\, \sqrt{t-t_{\rm l}}\, t_{\rm m}^{3/2} (t_{\rm l} - t_{\rm m})^{3/2}} \sum_{n=0}^{\infty} (-1)^n\, e^{-\frac{n^2 M^2}{4\,D\,(t-t_{\rm l})}} , \tag{C16}$$

where $\mathcal{N}_1(\epsilon_1)$ and $\mathcal{N}_2(\epsilon_2)$ are proportionality constants that are fixed by the overall normalization of the joint distribution. As in Eq. (B23) in the previous section, one can show that for proper normalization we must have the identities

$$\lim_{\epsilon_1 \to 0} \mathcal{N}_1(\epsilon_1)\, \frac{\epsilon_1^2}{D} = 1 \quad \text{and} \quad \lim_{\epsilon_2 \to 0} \mathcal{N}_2(\epsilon_2)\, \frac{\epsilon_2^2}{D} = 1 . \tag{C17}$$

Substituting these results in Eq. (C16) gives us a nice compact result for $t_{\rm l} > t_{\rm m}$

$$P(t_{\rm l}, t_{\rm m}, M|t) = \frac{\theta(t_{\rm l} - t_{\rm m})\, M^2}{2\,(\pi\, D)^{3/2}\, \sqrt{t-t_{\rm l}}\, t_{\rm m}^{3/2} (t_{\rm l} - t_{\rm m})^{3/2}} \sum_{n=0}^{\infty} (-1)^n\, e^{-\frac{n^2 M^2}{4\,D\,(t-t_{\rm l})}} . \tag{C18}$$

Finally, the integral over M can now be performed term by term to obtain the joint distribution $P_{13}^{>}(t_{\rm l}, t_{\rm m}|t)$ (with the superscript signifying $t_{\rm l} > t_{\rm m}$) which reads

$$P_{13}^{>}(t_{\rm l}, t_{\rm m}|t) = \frac{\theta(t_{\rm l} - t_{\rm m})}{\pi\, t_{\rm l}^{3/2} \sqrt{t-t_{\rm l}}} \sum_{n=0}^{\infty} \frac{(-1)^n}{(1+\alpha\, n^2)^{3/2}} \quad \text{where} \quad \alpha = \frac{t_{\rm m}\,(t_{\rm l} - t_{\rm m})}{t_{\rm l}\,(t-t_{\rm l})} . \tag{C19}$$

The case $t_{\rm l} < t_{\rm m}$. In this case, the process starts from 0 and arrives at $\epsilon_2 > 0$ at time $t_{\rm l}$, while staying below M–this is region I in Fig. (9). Then, in region II, the process starting at ϵ_2 at time $t_{\rm l}$, reaches at $M - \epsilon_1$ at time $t_{\rm m}$, while staying in the box $x \in [0, M]$ during the time interval $[t_{\rm l}, t_{\rm m}]$. Finally in region III, the process starting at $M - \epsilon_1$ at time $t_{\rm m}$ stays inside the box $x \in [0, M]$ during the rest of the time interval $[t_{\rm m}, t]$. As in the previos case, we will compute the propagators in each of these three regions separately to leading orders for small ϵ_1 and ϵ_2 and then take their product to compute the joint distribution $P(t_{\rm l}, t_{\rm m}, M|t)$ with $t_{\rm l} < t_{\rm m}$.

Interval I ($0 \le \tau \le t_{\rm l}$)**.** Here we can directly use the result in Eq. (C3) obtained via the method of images with the substitution $x = \epsilon_2$, $x_0 = 0$ and $\tau = t_{\rm l}$. This gives, after expanding in powers of ϵ_2 and keeping only the leading order term,

$$G_{\rm I} \approx \frac{\left[1 - e^{-M^2/D\, t_{\rm l}} \right]}{\sqrt{4\,\pi\, D\, t_{\rm l}}}\, \epsilon_2 . \tag{C20}$$

Interval II ($t_{\rm l} \le \tau \le t_{\rm m}$)**.** In this regime, the process moves in a box $x \in [0, M]$ starting from $\epsilon_2 > 0$ at time $t_{\rm l}$ and arriving at $M - \epsilon_2$ at time $t_{\rm m} > t_{\rm l}$. Hence we can use the box propagator in Eq. (C7) with the substitution $x = M - \epsilon_1$, $x_0 = \epsilon_2$ and $T = t_{\rm m} - t_{\rm l}$. Expanding again for small ϵ_1 and ϵ_2, we get to leading order

$$G_{\rm II} \approx \frac{2\pi^2 \epsilon_1\, \epsilon_2}{M^3} \sum_{n=1}^{\infty} (-1)^{n-1}\, n^2\, e^{-n^2\pi^2 D(t_{\rm m} - t_{\rm l})/M^2} . \tag{C21}$$

Interval III ($t_{\rm m} \le \tau \le t$)**.** In regime III, the process again moves in the box $x \in [0, M]$, starting at $M - \epsilon_1$ and surviving till time t, with absorbing boundary conditions at both $x = 0$ and $x = M$. Hence, we can again use the result for the survival probability $S(x_0, T|M)$ in Eq. (C8) with the substitution $x_0 = M - \epsilon_1$ and $T = t - t_{\rm m}$. Exapanding it for small ϵ_1, one gets to leading order the propagator for regime III

$$G_{\rm III} \approx \frac{4\epsilon_1}{M} \sum_{m=0}^{\infty} e^{-(2m+1)^2\pi^2 D(t-t_{\rm m})/M^2} . \tag{C22}$$

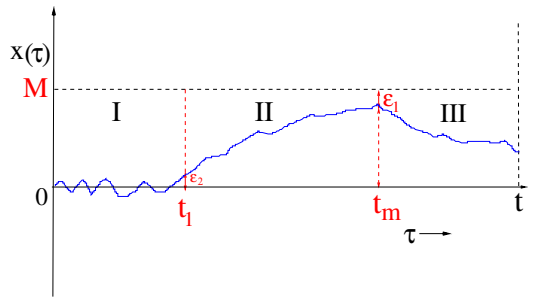

FIG. 9. A typical trajectory of a 1-d Brownian motion $x(\tau)$ of total duration t, starting at the origin $x(0) = 0$. The trajectory arrives at $\epsilon_2 > 0$ at time t_1 while staying below M and does not cross zero after time t_1. It also arrives at its maximum value $M - \epsilon_1$ at time t_m. We divide the total duration $[0, t]$ into three intervals: (I) the interval $[0, t_1]$ where the process, starting at the origin and staying below the level M, arrives at ϵ_2 at time t_1, (II) starting at ϵ_2 at time t_1 the process arrives at $M-\epsilon_1$ at time $t_m > t_1$, while staying below M and also above 0 and (III) starting at $M - \epsilon_1$ at time t_m, the process stays inside the box $[0, M]$ during the interval $[t_m, t]$. Eventually, we take the limits $\epsilon_1 \to 0$ and $\epsilon_2 \to 0$ at the end of the calculation.

Finally, taking the product of the three regimes, respectively in Eqs. (C20), (C21) and (C22), gives the joint distribution $P(t_1, t_m, M|t)$ for $t_1 < t_m$ as

$$P(t_1, t_m, M|t) = \frac{\theta(t_m - t_1)\, 8\pi^2\, D^2 \left(1 - e^{-M^2/Dt_1}\right)}{\sqrt{4\,\pi\, D\, t_1}\, M^4} \times \sum_{n,m=0}^{\infty} (-1)^{n-1} n^2\, e^{-\frac{\pi^2 D}{M^2}\left(n^2(t_m - t_1) + (2m+1)^2(t-t_m)\right)}\,, \tag{C23}$$

where we used exactly the same normalization as in Eq. (C17). We now have to integrate over M. For this we use the following identity

$$\int_0^\infty \frac{1}{M^4}\, e^{-b\,M^2 + a/M^2}\, dM = \frac{\sqrt{\pi}\left(1 + 2\sqrt{ab}\right)}{4a^{3/2}}\, e^{-2\sqrt{ab}} \tag{C24}$$

for $a > 0$, $b > 0$. We now integrate Eq. (C23) over M using the identity (C24) upon setting $a = \pi^2 D \left(n^2(t_m - t_1) + (2m+1)^2(t - t_m)\right)$ and $b = 1/(D\, t_1)$. Simplifying, we get the joint distribution $P_{13}^{<}(t_1, t_m|t)$ (with the superscript signifying $t_1 < t_m$) which reads

$$P_{13}^{<}(t_1, t_m|t) = \frac{\theta(t_m - t_1)}{\pi\, t_1^2} \times \sum_{n,m=0}^{\infty} \frac{(-1)^{n-1}\, n^2}{\gamma_{n,m}^{3/2}} \left[1 - \left(1 + 2\,\pi\,\sqrt{\gamma_{n,m}}\right) e^{-2\,\pi\,\sqrt{\gamma_{n,m}}}\right], \tag{C25}$$

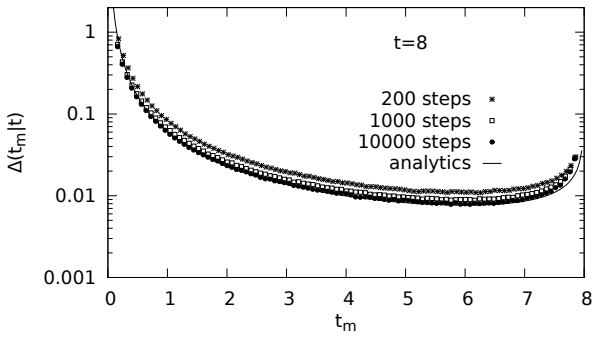

FIG. 10. The jump $\Delta(t_m, t)$ in the joint PDF joint $P(t_m, t_1|t)$ as $t_1 \to t_m^+$, plotted as a function of t_m for fixed $t = 8$. The symbols show simulation results with increasing number of steps and the solid line represents the analytical result in Eq. (C29). The simulation results appraoch the analytical formula as the number of steps increases.

where

$$\gamma_{n,m} = \frac{\left[n^2(t_m - t_1) + (2m+1)^2(t - t_m)\right]}{t_1}\,. \tag{C26}$$

Adding Eqs. (C19) and (C25), we get our final answer for the joint distribution $P_{13}(t_1, t_m|t) = P_{13}^{>}(t_1, t_m|t) + P_{13}^{<}(t_1, t_m|t)$ that results in (12)

We have investigated the asymmetric behavior of the joint PDF for $t_1 = t_m - \epsilon$ and $t_1 = t_m + \epsilon$ as $\epsilon \to 0$. By analysing Eq. (12) we find the following results as t_1 approches t_m from above and below,

$$P_{13}(t_1, t_m|t) \approx \begin{cases} \frac{1}{2\,\pi\, t_m^{3/2}\,\sqrt{t - t_m}}\,, & \text{as} \quad t_1 \to t_m^+ \\ C(t_m, t)\,(t_m - t_1)^{-7/4}\, \exp\left[-\frac{\pi}{\sqrt{t_m - t_1}}\sqrt{\frac{t - t_m}{t_m}}\right] & \text{as} \quad t_1 \to t_m^-\,, \end{cases} \tag{C27}$$

where the amplitude $C(t_m, t)$ can also be computed explicitly and is given by

$$C(t_m, t) = \frac{1}{\sqrt{2}\, t_m^2} \left(\frac{t - t_m}{t_m}\right)^{1/4} \times \left[1 - \left[1 + 2\,\pi\,\sqrt{\frac{t - t_m}{t_m}}\right] e^{-2\,\pi\,\sqrt{\frac{t-t_m}{t_m}}}\right]. \tag{C28}$$

Thus, as $t_1 \to t_{\rm m}$ from below, the joint distribution vanishes extremely rapidly (with an essential singularity as seen in Eq. (C27)). In contrast, as $t_1 \to t_{\rm m}$ from above, it approaches a nonzero constant given in Eq. (C27). Hence the discontinuity

$$\Delta(t_{\rm m},t) = P_{13}(t_1=t_{\rm m}^+,t_{\rm m}|t) - P(t_1=t_{\rm m}^-,t_{\rm m}|t) = \frac{1}{2\,\pi\,t_{\rm m}^{3/2}\,\sqrt{t-t_{\rm m}}}\,, \tag{C29}$$

is a non-monotonic function of $t_{\rm m}$ for fixed t. In Fig. (10) we plot $\Delta(t_{\rm m},t)$ as a function of $t_{\rm m}$ for fixed t and compare it to simulations. The agreement between the analytical result in Eq. (C29) and the simulation results is excellent.

Finally, although in principle possible, computing the joint moments of t_1 and $t_{\rm m}$ from the joint distribution seems a bit hard compared to the two previous cases. Thus, we did not perform this task.

Appendix D: Feynman-Kac method to compute the distribution of the occupation time for a bridge of duration t

Consider a Brownian motion of duration t_1, starting at the origin $x(0)=0$ and arriving at x at time t_1. We will finally set $x=0$ for our Brownian bridge. Let $t_{\rm o}=\int_0^{t_1}\theta\left(x(\tau)\right)\,d\tau$ denote the occupation time for this bridge of duration t_1. Let us denote the joint PDF of $t_{\rm o}$ and the final position x at time t_1 by $P(x,t_{\rm o}|t_1)$. Let us now take the Laplace transform with respect to $t_{\rm o}$ and define

$$\tilde{P}_p(x|t_1)=\int_0^\infty dt_{\rm o}\,e^{-p\,t_{\rm o}}\,P(x,t_{\rm o}|t_1)\,. \tag{D1}$$

Note that by definition $t_{\rm o}\le t_1$, hence the PDF $P(x,t_{\rm o}|t_1)$ must vanish for $t_{\rm o}\ge t_1$, i.e., the upper limit of the integral in Eq. (D1) is strictly t_1. Now, $\tilde{P}_p(x|t_1)$ satisfies the Feynman-Kac equation that reads [104]

$$\frac{\partial\tilde{P}_p}{\partial t_1}=D\,\frac{\partial^2\tilde{P}_p}{\partial x^2}-p\,\theta(x)\,\tilde{P}_p(x|t_1)\,, \tag{D2}$$

with the initial condition $\tilde{P}_p(x|t_1=0)=\delta(x)$. The last condition comes from the fact that when $t_1=0$, the final position x must coincide with the initial position (since the particle didn't evolve). Since initially the particle is at the origin, clearly then $\tilde{P}_p(x|t_1=0)=\delta(x)$.

To solve the partial differential equation (PDE) (D2), it is convenient further to take a Laplace transform with respect to t_1 and define

$$R_p(x,s)=\int_0^\infty dt_1\,e^{-s\,t_1}\,\tilde{P}_p(x|t_1)\,. \tag{D3}$$

Taking Laplace transform of Eq. (D2) with respect to t_1 and using the initial condition, we obtain an ordinary second order differential equation for $R_p(x,s)$

$$D\,\frac{d^2R_p}{dx^2}-\left(s+p\,\theta(x)\right)\,R_p=-\delta(x)\,, \tag{D4}$$

subject to the boundary conditions: $R_p(x\to\pm\infty,s)=0$. To solve this differential equation we solve it for $x<0$ and $x>0$ separately and then match the solution at $x=0$. For $x<0$, the solution is simply $R_p(x,s)=A\,e^{\sqrt{s/D}\,x}$ where A is a constant. Note that we have used the boundary condition $R_p(x\to-\infty,s)=0$ to discard the exponentially growing solution. Similarly, for $x>0$, we get $P_p(x,s)=A\,e^{-\sqrt{(s+p)/D}\,x}$, where we used $R_p(x\to\infty,s)=0$ and the continuity of the solution at $x=0$. Finally, the unknown constant A can be fixed by noting the jump (in the derivative at $x=0$) condition (follows by integrating Eq. (D4) across $x=0$): $R_p'(x\to0^+,s)-R_p'(x\to0^-,s)=-1/D$. This gives

$$A=\frac{1}{\sqrt{D}\,\left(\sqrt{s}+\sqrt{s+p}\right)}\,. \tag{D5}$$

This gives the complete solution $R_p(x,s)$ in the Laplace space. However, we are interested only in the bridge case when $x=0$. Hence, we have

$$\int_0^\infty dt_1\,e^{-s\,t_1}\int_0^{t_1}dt_{\rm o}\,e^{-p\,t_{\rm o}}\,P(x=0,t_{\rm o}|t_1)= R_p(x=0,s)=A=\frac{1}{\sqrt{D}\,\left(\sqrt{s}+\sqrt{s+p}\right)}\,. \tag{D6}$$

Fortunately, the double Laplace transform can be exactly inverted and we get for the interval I

$$P(x=0,t_{\rm o}|t_1)=\frac{1}{\sqrt{4\,\pi\,D\,t_1^3}}\,\theta\left(t_1-t_{\rm o}\right)\,. \tag{D7}$$

Thus, interestingly the distribution is flat as a function of $t_{\rm o}$. The explicit dependence on $t_{\rm o}$ is only in the upper bound (through the theta function). We are not done yet. Because $P(x=0,t_{\rm o}|t_1)$ is the joint probability that the process in $[0,t_1]$ has occupation time $t_{\rm o}$ and that the end position of the process is at $x=0$. To calculate the conditional PDF of $t_{\rm o}$ (given t_1), we need to divide it by the probability that the process reaches $x=0$ at time t_1, which is simply $1/\sqrt{4\,\pi\,D\,t_1}$ for a Brownian motion of duration t_1. Hence, dividing Eq. (D7) by $1/\sqrt{4\,\pi\,D\,t_1}$, we finally get the PDF of $t_{\rm o}$, given t_1, as simply a uniform distribution

$$p(t_{\rm o},t_1)=\frac{1}{t_1}\,\theta\left(t_1-t_{\rm o}\right)\,. \tag{D8}$$

[1] P. Fornasini, *The Uncertainty in Physical Measurements — An Introduction to Data Analysis in the Physics Laboratory* (Springer, New York, 2008).

[2] V. L. Smith, Amer. Economic Rev. **66**, 274 (1976), ISSN 00028282.

[3] D. Houle, C. Pélabon, G. Wagner, and T. Hansen, Quarterly Rev.of Biol. **86**, 3 (2011).

[4] P. D. Delmas, Osteoporosis Intern. **9**, S33 (1999), ISSN 1433-2965.

[5] L. Bennani, F. Allali, S. Rostom, I. Hmamouchi, H. Khazzani, L. El Mansouri, L. Ichchou, F. Z. Abourazzak, R. Abouqal, and N. Hajjaj-Hassouni, Clinical Rheumatology **28**, 1283 (2009), ISSN 1434-9949.

[6] T. A. Hillier, L. Lui, D. M. Kado, E. LeBlanc, K. K. Vesco, D. C. Bauer, J. A. Cauley, K. E. Ensrud, D. M. Black, M. C. Hochberg, et al., J. Bone Mineral Res. **27**, 153 (2012), ISSN 0884-0431.

[7] W. Pluskiewicz, P. Adamczyk, A. Werner, M. Bach, and B. Drozdzowska, Biomedicines **11** (2023), ISSN 2227-9059.

[8] D. M. Ragan, *Structural Geology* (Cambridge University Press, Cambridge, 2012).

[9] S. D. Sloan, G. P. Tsoflias, D. W. Steeples, and P. D. Vincent, J. Appl. Geophys. **62**, 281 (2007), ISSN 0926-9851.

[10] H. Yuan, A. Z. Abdu, and L. Nielsen, Geophys. **88**, MR141 (2023), ISSN 0016-8033.

[11] J. A. Hildebrand, S. M. Wiggins, J. L. Driver, and M. R. Waters, Archaeological Prospection **14**, 245 (2007).

[12] R. Serfozo, *Basics of Applied Stochastic Processes* (Springer, Berlin, Heidelberg, 2009).

[13] W. Feller, *Introduction to Probability Theory and Its Applications*, John Wiley & Sons, New York (1957).

[14] P. Mörters, Y. Peres, Brownian motion, Vol. 30, Cam- bridge University Press, (2010).

[15] R. M. Mazo, *Brownian Motion: Fluctuations, Dynamics, and Applications* (Oxford University Press, Oxford, 2008).

[16] P. Doyle and J. Snell, *Random walks and electric networks* (Math. Ass. Amer., Washington DC, 1984).

[17] J. Baz and G. Chacko, *Financial derivatives: pricing, applications, and mathematics* (Cambridge University Press, 2004)

[18] A. Hirsa and S. N. Neftci, *An introduction to the mathematics of financial derivatives* (Academic Press, Amsterdam, 2014).

[19] F. Schweitzer, *Browning Agents and Active Particles : Collective Dynamics in the Natural and Social Sciences* (Springer, Berlin, Heidelberg, 2007).

[20] S. Redner, *A guide to first-passage processes*, Cambridge University Press, Cambridge, 2001.

[21] S. N. Majumdar, Curr. Sci. 89, 2075 (2005).

[22] S. N. Majumdar, Physica A **389**, 4299 (2010).

[23] A. J. Bray, S. N. Majumdar, and G. Schehr, Adv. in Phys. **62**, 225 (2013).

[24] L. A. Shepp, J. Appl. Proba. **16**, 423 (1979).

[25] E. Buffet, J. Appl. Math. Stoch. Anal. 16, 201 (2003).

[26] J. Randon-Furling and S. N. Majumdar, J. Stat. Mech. P10008 (2007).

[27] S. N. Majumdar, J. Randon-Furling, M. J. Kearney, M. Yor, J. Phys. A: Math. Theor. **41**, 365005 (2008)

[28] S. N. Majumdar, J.-P. Bouchaud, Quant. Fin. 8, 753 (2008).

[29] S.N. Majumdar, A. Comtet, J. Randon-Furling, J. Stat. Phys. 138, 955 (2010).

[30] G. Schehr and P. Le Doussal, J. Stat. Mech. P01009 (2010).

[31] J. Rambeau and G. Schehr, Phys. Rev. E **83**, 061146 (2011).

[32] F. Mori, S. N. Majumdar, G. Schehr, Phys. Rev. Lett., **123**, 200201 (2019).

[33] F. Mori, S. N. Majumdar, and G. Schehr, Phys. Rev. E, **101**, 052111 (2020).

[34] P. Lévy, Compositio Mathematica **7**, 283 (1940).

[35] E. Sparre Andersen, Math. Scand. **1**, 263 (1954).

[36] J. Lamperti, Trans. Amer. Math. Soc. **88**, 380 (1958).

[37] C. Godrèche and J. M. Luck, J. Stat. Phys. **104**, 489 (2001), ISSN 1572-9613.

[38] S. Burov, E. Barkai, Phys. Rev. Lett. **107**, 170601 (2011).

[39] F. den Hollander, S. N. Majumdar, J. M. Meylahn, and H. Touchette, J. Phys. A: Math. Theor. **52**, 175001 (2019).

[40] A. Dhar and S. N. Majumdar, Phys. Rev. E **59**, 6413 (1999).

[41] G. De Smedt, C. Godrèche, and J. M. Luck, J. Phys. A: Math. Gen. **34**, 1247 (2001).

[42] T. J. Newman and Z. Toroczkai, Phys. Rev. E **58**, R2685 (1998).

[43] J.-M. Drouffe and C. Godrèche, J. Phys. A **31**, 9801 (1998).

[44] Z. Toroczkai, T. J. Newman, and S. Das Sarma, Phys. Rev. E **60**, R1115 (1999).

[45] A. Baldassarri, J.-P. Bouchaud, I. Dornic, and C. Godrèche, Phys.Rev. E **59**, R20 (1999).

[46] J. T. Cox and D. Griffeath, Annals Prob. **11**, 876 (1983), ISSN 00911798.

[47] G. Margolin and E. Barkai, Phys. Rev. Lett. **94**, 080601 (2005).

[48] S. N. Majumdar and A. Comtet, Phys. Rev. Lett. **89**, 060601 (2002).

[49] S. Sabhapandit, S. N. Majumdar, and A. Comtet, Phys. Rev. E **73**, 051102 (2006).

[50] M. Radice, M. Onofri, R. Artuso, and G. Pozzoli, Phys. Rev. E **101**, 042103 (2020).

[51] T. Kay and L. Giuggioli, J. Phys. A: Math. Theor. **56**, 345002 (2023).

[52] S. N. Majumdar and D. S. Dean, Phys. Rev. E **66**, 041102 (2002).

[53] G. Bel and E. Barkai, Phys. Rev. Lett. **94**, 240602 (2005).

[54] E. Barkai, J. Stat. Phys. **123**, 883 (2006).

[55] G, Del Vecchio Del Vecchio and S. N. Majumdar, J. Stat. Mech. 023207 (2025).

[56] T. Sadhu, M. Delorme, K. J. Wiese, Phys. Rev. Lett. **120**, 040603 (2018).

[57] H. J. O. Boutcheng, T. B. Bouetou, T. W. Burkhardt, A. Rosso, A. Zoia, K. T. Crepin, J. Stat. Mech. 053213 (2016).

[58] P. Singh and A. Kundu, J. Stat. Mech. 083205 (2019).

[59] P. C. Bressloff, Phys. Rev. E **102**, 042135 (2020).

[60] S. Mukherjee and N. R. Smith, Phys. Rev. E **107**, 064133 (2023).

[61] X. Fang, H. L. Gan, S. Holmes, H. Huang, E. Peköz, A. Röllin, and W. Tang, J. Appl. Prob. **58**, 851–867 (2021).

[62] I. N. Burenev, S. N. Majumdar, A. Rosso, Phys. Rev. E, **109**, 044150 (2024).

[63] X. Brokmann, J.-P. Hermier, G. Messin, P. Desbiolles, J.-P. Bouchaud, and M. Dahan, Phys. Rev. Lett. **90**, 120601 (2003).

[64] F. D. Stefani, J. P. Hoogenboom, and E. Barkai, Physics Today **62** (2), 34 (2009).

[65] A. C. Barato, E. Roldán, I. A. Martínez, and S. Pigolotti, Phys. Rev. Lett. **121**, 090601 (2018).

[66] V. G. Ramesh, K. J. H. Peters, and S. R. K. Rodriguez, Phys. Rev. Lett. **132**, 133801 (2024).

[67] S. N. Majumdar, A. Pal, and G. Schehr, Phys. Rep. **840**, 1 (2020).

[68] S. N. Majumdar and G. Schehr, *Statistics of Extremes and Records in Random Sequences*, Oxford University Press, (2024).

[69] S. N. Majumdar, A. Rosso, and A. Zoia, Phys. Rev. Lett. **104**, 020602 (2010).

[70] F. Mori, S. N. Majumdar, and G. Schehr, Europhys. Lett. **135**, 30003 (2021).

[71] S. N. Majumdar, A. Rosso, and A. Zoia, J. Phys. A: Math.

Theor. **43**, 115001 (2010).
[72] P. Singh, Phys. Rev. E **105**, 024113 (2022).
[73] M. Delorme, K. J. Wiese, Phys. Rev. E **94**, 052105 (2016).
[74] P. Singh and A. Pal, Phys. Rev. E **103**, 052119 (2021).
[75] F. Mori, S. N. Majumdar, and G. Schehr, Phys. Rev. E **106**, 054110 (2022).
[76] J. Randon-Furling, S. N. Majumdar, and A. Comtet, Phys. Rev. Lett. **103**, 140602 (2009).
[77] S. N. Majumdar, A. Comtet, and J. Randon-Furling, J. Stat. Phys. **138**, 955 (2010).
[78] A. Reymbaut, S. N. Majumdar, and A. Rosso, J. Phys. A: Math. Theor. **44**, 415001 (2011).
[79] E. Dumonteil, S. N. Majumdar, A. Rosso, and A. Zoia, Proc. Natl. Aca. Sci. U. S. A., **110**, 4239 (2013).
[80] A. K. Hartmann, S. N. Majumdar, H. Schawe, and G. Schehr, J. Stat. Mech. 053401 (2020).
[81] S. N. Majumdar, F. Mori, H. Schawe, and G. Schehr, Phys. Rev. E **103**, 022135 (2021).
[82] P. Singh, A. Kundu, S. N. Majumdar, and H. Schawe, J. Phys. A.: Math. Theor. **55**, 225001 (2022).
[83] C. Dale and R. Workman, Financ. Analysts J. **36**, 71 (1980).
[84] R. Chicheportiche and J.-P. Bouchaud, in: R. Metzler, G. Oshanin, and S. Redner (eds.), *First-Passage Phenomena and Their Applications*, 447 (World Scientific, Singapore 2014).
[85] A. Clauset, M. Kogan, and S. Redner, Phys. Rev. E **91**, 062815 (2015).
[86] J. D. Bao and Y. Jia, J. Stat. Phys. **123**, 861 (2006).
[87] A. Comtet, F. Cornu, and G. Schehr, J. Stat. Phys. **181**, 1565 (2020).
[88] B. H. Leung, IEEE Trans. Circuits Syst. I: Regular Papers, **51**, 471 (2004).
[89] S. Robson, B. Leung, and G. Gong, IEEE Trans. Circuits Syst. II: Express Briefs **61**(12), 937 (2014).
[90] J. D. Bao, and Y. Jia, Phys. Rev. C **69**, 027602 (2004).
[91] C.-O. Hwang and J. A. Given, Phys. Rev. E **74**, 027701 (2006).
[92] U. Yu, Y.-M. Lee, and C.-O. Hwang, J. Sci. Comput. **88**, 82 (2021).
[93] C. T. Barkar and M. J. Newby, Reliability Engineering & System Safety, **94**, 33 (2009).
[94] A. Nikeghbali and E. Platen, Finance Stoch. **17**, 615 (2013).
[95] M. H. Bin Azami, N. C. Orger, V. H. Schulz, T. Oshiro, and M. Cho, Remote Sensing **14** (2022).
[96] V. Mazák, Mammalian Species pp. 1–8 (1981), ISSN 0076-3519.
[97] S.N. Majumdar and A. Comtet, Phys. Rev. Lett., **92**, 225501 (2004).
[98] S.N. Majumdar and A. Comtet, J. Stat. Phys. **119**, 777 (2005).
[99] A. Perret, A. Comtet, S. N. Majumdar, G. Schehr, Phys. Rev. Lett., **111**, 240601 (2013).
[100] A. K. Hartmann, *Big Practical Guide to Computer Simulations* (World Scientific, Singapore 2015).
[101] B. Walter and K. J. Wiese, Phys. Rev. E **101**, 043312 (2020).
[102] MPFR multi precision floating point library, `https://www.mpfr.org/`
[103] W. Feller, *An Introduction to Probability Theory and its Applications* (New York: Wiley, 1957).
[104] S. N. Majumdar, Current Science, **89**, 2076 (2005).
[105] A. Perret, A. Comtet, S. N. Majumdar and G. Schehr, J. Stat. Phys., **161**, 1112 (2015).
[106] F. Mori, S. N. Majumdar, G. Schehr, Phys. Rev. Lett., **123**, 200201 (2019).
[107] F. Mori, S. N. Majumdar, and G. Schehr, Phys. Rev. E, **101**, 052111 (2020).
[108] S.N. Majumdar and A.J. Bray, Phys. Rev. E **65**, 051112 (2002).